CrossMark click for updates



# Let-7 family of microRNA is required for maturation and adult-like metabolism in stem cell-derived cardiomyocytes

Kavitha T. Kuppusamy[a,b], Daniel C. Jones[c], Henrik Sperber[a,b,d], Anup Madan[e], Karin A. Fischer[a,b], Marita L. Rodriguez[f], Lil Pabon[a,g,h], Wei-Zhong Zhu[a,g,h], Nathaniel L. Tulloch[a,g,h], Xiulan Yang[a,g,h], Nathan J. Sniadecki[f,i], Michael A. Laflamme[a,g,h], Walter L. Ruzzo[c,j,k], Charles E. Murry[a,g,h,i,l], and Hannele Ruohola-Baker[a,b,i,j,m,1]

[a]Institute for Stem Cell and Regenerative Medicine, Seattle, WA 98109; Departments of [b]Biochemistry, [c]Computer Science and Engineering, and [d]Chemistry, University of Washington, Seattle, WA 98195; [e]LabCorp Genomic Services, Seattle, WA 98109; [f]Department of Mechanical Engineering, [g]Department of Pathology, [h]Center for Cardiovascular Biology, [i]Department of Bioengineering, and [j]Department of Genome Sciences, University of Washington, Seattle, WA 98195; [k]Fred Hutchinson Cancer Research Center, Seattle, WA 98109; and [l]Department of Medicine/Cardiology and [m]Department of Biology, University of Washington, Seattle, WA 98195

Edited by Eric N. Olson, University of Texas Southwestern Medical Center, Dallas, TX, and approved April 14, 2015 (received for review December 18, 2014)

**In metazoans, transition from fetal to adult heart is accompanied by a switch in energy metabolism-glycolysis to fatty acid oxidation. The molecular factors regulating this metabolic switch remain largely unexplored. We first demonstrate that the molecular signatures in 1-year (y) matured human embryonic stem cell-derived cardiomyocytes (hESC-CMs) are similar to those seen in in vivo-derived mature cardiac tissues, thus making them an excellent model to study human cardiac maturation. We further show that let-7 is the most highly up-regulated microRNA (miRNA) family during in vitro human cardiac maturation. Gain- and loss-of-function analyses of let-7g in hESC-CMs demonstrate it is both required and sufficient for maturation, but not for early differentiation of CMs. Overexpression of let-7 family members in hESC-CMs enhances cell size, sarcomere length, force of contraction, and respiratory capacity. Interestingly, large-scale expression data, target analysis, and metabolic flux assays suggest this let-7–driven CM maturation could be a result of down-regulation of the phosphoinositide 3 kinase (PI3K)/AKT protein kinase/insulin pathway and an up-regulation of fatty acid metabolism. These results indicate let-7 is an important mediator in augmenting metabolic energetics in maturing CMs. Promoting maturation of hESC-CMs with let-7 overexpression will be highly significant for basic and applied research.**

let-7 | cardiac maturation | hESC-cardiomyocyte | metabolism | microRNA

Several coronary heart diseases (CHDs) are characterized by cardiac dysfunctions predominantly manifested during cardiac maturation (1, 2). Dramatic changes in energy metabolism occur during this postnatal cardiac maturation (3). At early embryonic development, glycolysis is a major source of energy for cardiomyocytes (CMs) (4, 5). However, as the cardiomyocytes mature, mitochondrial oxidative metabolism increases with fatty acid oxidation, providing 90% of the heart's energy demands (6–8). This switch in cardiac metabolism has been shown to have important implications during in vivo cardiac maturation (9). In contrast to the relatively advanced knowledge of the genetic network that contributes to heart development during embryogenesis (10, 11), molecular factors that regulate peri- and postnatal cardiac maturation, particularly in relation to the metabolic switch, remain largely unclear. So far, studies to understand the transition of the glycolysis-dependent fetal heart to oxidative metabolism in the adult heart have been mostly related to the peroxisome proliferator-activated receptor (PPAR)/estrogen-related receptor/PPARγ coactivator-1α circuit (7, 8, 12). However, it is currently unknown what other factors act upstream or in synergy with this pathway in controlling cardiac energetics.

miRNAs have emerged as key factors in controlling the complex regulatory network in a developing heart (13). Genetic studies that enrich or deplete miRNAs in specific cardiac tissue types and large-scale gene expression studies have demonstrated that they achieve such complex control at the level of cardiac gene expression (14–16). We sought to determine whether these small noncoding RNAs have an important role during cardiac maturation, specifically in relation to cardiac energetics. The in vitro-generated human embryonic stem cell-derived CMs (hESC-CMs), despite displaying several functional and physiological similarities to the CMs in the developing heart, are in a fetal state with respect to their ion channel expression and electrophysiological activity, as well as their metabolic phenotype (17–21). In this study, we therefore have used hESC-CMs as a powerful platform to understand and elucidate cardiac maturation. Using large-scale transcriptome analysis, we first show that molecular signature patterns of hESC-CMs taken through 1 y of culturing for cardiac maturation reflect in vivo cardiac maturation. Furthermore, large-scale miRNA sequencing of in vitro-derived mature hESC-CMs reveals several key differentially regulated miRNAs and miRNA families. Target analysis using miRNA and mRNA datasets from mature CMs indicates that the let-7 family, which is one of the most highly up-regulated families, targets several key genes in the PI3K/AKT/insulin pathway during cardiac maturation. Because

## Significance

**The adult human heart is incapable of significant regeneration after injury. Human embryonic stem cells (hESCs) have the capacity to generate an unlimited number of cardiomyocytes (CMs). However, hESC-derived CMs (hESC-CMs) are at a fetal state with respect to their functional and physiological characteristics, diminishing their utility for modeling adult-related heart disease and therapeutic screening. Thus, the potential for hESC-CMs may improve immensely in cardiac-related therapeutic applications if factors that drive their maturation are uncovered. In this study, we show that members of let-7 miRNA family control CM metabolism, cell size, and force contractility, making them one of the best factors identified to date in promoting maturity of stem cell derivatives.**

Author contributions: K.T.K., D.C.J., M.A.L., W.L.R., C.E.M., and H.R.-B. designed research; K.T.K., A.M., K.A.F., M.L.R., L.P., W.-Z.Z., and X.Y. performed research; K.T.K., D.C.J., N.L.T., N.J.S., M.A.L., and W.L.R. contributed new reagents/analytic tools; K.T.K. and H.R.-B. analyzed data; D.C.J., H.S., and W.L.R. performed bioinformatics analysis; and K.T.K. and H.R.-B. wrote the paper.

The authors declare no conflict of interest.

This article is a PNAS Direct Submission.

Data deposition: The data reported in this paper have been deposited in the Gene Expression Omnibus (GEO) database, www.ncbi.nlm.nih.gov/geo (accession no. GSE62913).

[1]To whom correspondence should be addressed. Email: hannele@uw.edu.

This article contains supporting information online at www.pnas.org/lookup/suppl/doi:10.1073/pnas.1424042112/-/DCSupplemental.

the let-7 family has been previously associated with energy metabolism (22, 23), it was chosen as a prime candidate for further analyses. Knock-down (KD) of let-7 results in a significant decrease in a number of maturation parameters such as CM size, area, sarcomere length, and expression of several cardiac maturation markers. Overexpression of selected members of the let-7 family for just 2 wk in hESC-CMs significantly increases cell size, sarcomere length, contractile force, and action potential duration. More importantly, the overexpression (OE) of let-7 in CMs exhibit higher respiratory capacity and increased efficiency in using palmitate as an energy source, thus strongly implying a metabolic transition in these cells. This switch is synchronized with a significant down-regulation of a number of let-7 target genes in the PI3K/AKT/insulin pathway and other key regulators such as the histone methyl transferase enhancer of zeste homolog 2 (EZH2), suggesting let-7 acts as a global regulator to bring about the metabolic and functional changes required during cardiac maturation. Finally, repression of insulin receptor substrate 2 (IRS2) and EZH2 in CMs mimics the effect of let-7 OE, suggesting these targets could be important components of a let-7-driven maturation pathway. Altogether, our results indicate the let-7 family as a novel endogenous regulator that can simultaneously accelerate maturation and adult-like metabolism in human cardiac tissue.

## Results

**In Vitro Cardiac Maturation Physiologically Simulates in Vivo Cardiac Maturation.** To examine whether hESC-CMs can be used as a model to study CM maturation, we adopted two different maturation protocols for hESC (H7)-CMs: 3D engineered heart tissue culture and prolonged 2D culture conditions (Fig. 1*A*). 3D engineered heart tissue was generated in gels of type I collagen and mechanically conditioned via static stress for 2 wk by fixing the ends of the constructs between two posts (termed cEHT here, for conditioned engineered heart tissue) (24). Previous reports have shown that prolonged culturing of hESC-CMs for up to 1 y can result in a tightly packed and parallel array of myofibrils with mature Z, A, H, I, and M bands (25). Thus, in the second protocol we adopted, standard 2D CMs were subjected to prolonged culturing (13.5 mo, termed 1y-CM). In the current investigation, CM

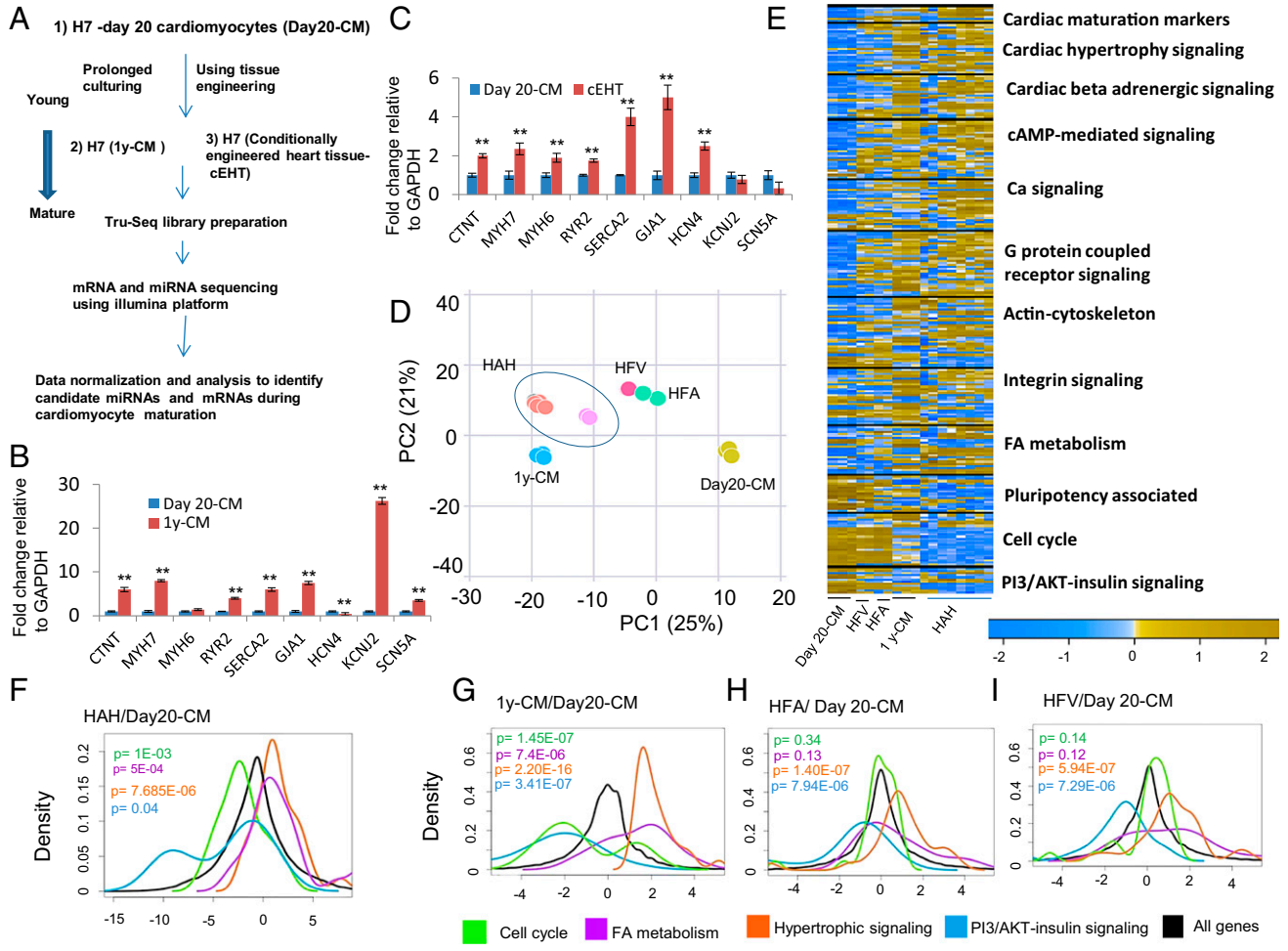


**Fig. 1.** The molecular signatures of in vitro cardiac maturation reflect in vivo cardiac maturation. (*A*) Schematic representation of large-scale mRNA and miRNA sequencing using Illumina platform from day 20-CMs and in vitro-matured CMs derived from hESC (H7). (*B* and *C*) qPCR analysis of maturation markers in day 20-CMs and in vitro-matured CMs. Means ± SEM are shown. $^{**}P \leq 0.05$ (Student's *t* test). (*D*) 2D principal component analysis using genomewide expression data for day 20-CMs, 1y-CMs, HAH, HFA, and HFV samples attained using R. (*E*) Heat map depicting changes in gene expression of 12 different pathways between day 20-CMs, 1y-CMs, HAH, HFA, and HFV samples attained using R. The rows reflect read counts and are standardized individually and colored according to the Z score. Yellow and blue represent up- and down-regulation, respectively. (*F–I*) Density plots using R generated with fold change expression of genes from four representative categories for HAH (*F*), 1y-CM (*G*), HFA (*H*), and HFV (*I*) relative to gene expression of day 20-CMs. *X* axis indicates $\log_2$ fold change in gene expression. Black line indicates expression of all genes. Colored lines toward the left and right side of the black line indicate down-regulation and up-regulation of pathways, respectively. All experiments were repeated at least three times.

populations with higher than 70% purity assessed by flow cytometry for cardiac troponin T positive ($cTnT^+$) cells were used for all assays (*SI Appendix*, Fig. S1). Quantitative PCR analysis of known cardiac markers further validated the maturation process (Fig. 1 *B* and *C*). To further verify the extent of maturation of CMs generated by in vitro methods, we used large-scale sequencing, using an Illumina platform, to compare the mRNA expression profiles between day 20-CMs and 1 y-CMs in relation to human adult heart (HAH) samples (see more details on HAH in *Materials and Methods* and *SI Appendix*) and 3-mo-old human fetal ventricular (HFV) and atrial (HFA) samples (26) (Fig. 1*E* and Dataset S1). 2D principal component analysis (2D PCA) of all genes for all of the samples clearly separates 1y-CMs and HAH samples the farthest from day 20-CMs while placing the HFA and HFV samples in the middle in the principal component 1 (PC1) axis (Fig. 1*D*). Examination of the transcript levels of all significantly regulated genes [$P \leq 0.001$ and fold change (FC) $\geq 2$] in the abovementioned samples, using Ingenuity Pathway Analysis (IPA), revealed several interesting patterns and groups across the different samples. Cardiac maturation is known to improve Ca handling (27), fatty acid metabolism (9, 28), and sarcomere organization (29) and results in the down-regulation of glucose metabolism/insulin signaling (30), cell proliferation (31), and pluripotency. Twelve categories reflecting these parameters are presented as a heat map (Fig. 1*E* and Dataset S2). Most categories show the same trend of up- or down-regulation between 1y-CMs and HAH, suggesting that several pathways known to be critical during in vivo heart development are also coregulated during in vitro cardiac maturation (Fig. 1*E*). A more in-depth evaluation of the data using density plots revealed that pathways related to hypertrophic signaling, sarcomere organization (actin cytoskeleton), calcium, and cAMP-mediated signaling (27) and integrin signaling were significantly up-regulated ($P \leq 0.01$) in both HAH and 1y-CM samples, suggesting in vitro maturation processes physiologically simulate the in vivo cardiac maturation (Fig. 1 *E–I* and *SI Appendix*, Fig. S2 *A–H*). Previous studies have shown that CMs rapidly proliferate during fetal life (31). However, a vast majority of postnatal human CMs do not proliferate, although they are capable of DNA synthesis without nuclear division or nuclear division without cytokinesis, thereby increasing in ploidy (8N) and size (hypertrophy) (31–33). Consistent with these data, a number of cell cycle-related genes were still up-regulated in our 3-mo-old HFV and HFA samples (Fig. 1*E*) and did not show a significant down-regulation (Fig. 1 *H* and *I*). In contrast, in both HAH and 1y-CMs, the cell cycle genes were significantly down-regulated. (Fig. 1 *F* and *G*).

In animal models, CMs are known to shift their metabolism from glycolysis to fatty acid oxidation during postnatal cardiac maturation. This is well documented in in vivo studies using murine and rabbit models (3, 34, 35). Furthermore, accumulating molecular and clinical data in humans support a similar transition from glycolysis to fatty acid metabolism as the CMs undergo postnatal maturation (36, 37). Consistent with this, although the HFA and HFV samples do not show an increase in fatty acid metabolism (Fig. 1 *E*, *H*, and *I*), several genes in the fatty acid metabolism pathway are up-regulated in both 1y-CMs and HAH samples (Fig. 1 *E*, *F*, and *G* and Dataset S2). Interestingly, in parallel to increased fatty acid metabolism, a down-regulation of several genes in the PI3/AKT/insulin pathway was observed in the 1y-CMs and HAH (Fig. 1 *E–G* and Dataset S2), suggesting a reduced use of glucose for their metabolic needs. These profiling data together indicate that in vitro maturation of hESC-CMs results in CMs that possess molecular signatures similar to those seen in postnatal CMs, and thus can be used as an excellent model to elucidate novel regulators during cardiac maturation. The effect of long-term culturing on cardiac maturation was also analyzed in the IMR90-induced pluripotent stem cell line and the overall gene expression of the IMR90 iPSC line was very similar to that derived from the H7 line (*SI Appendix*, Fig. S3). It was intriguing to see that despite the heterogeneity in the composition of human fetal and adult heart samples in comparison with the in vitro-matured CMs, the overall behavior in the trends of the various pathways was still consistent with what is known during cardiac maturation.

**Let-7 Family of miRNAs Is Highly Expressed in hESC-CMs Matured in the Dish.** Because miRNA patterns in cEHTs and 1y-CMs should reflect the miRNA pattern changes observed during cardiac maturation, we used an Illumina high-throughput miRNA sequencing platform to elucidate miRNAs that are highly enriched in these samples compared with day 20-CMs (Fig. 2*A* and Datasets S3 and S4). Approximately 600 miRNAs were identified with deducible read counts (Fig. 2*A*) from each of the two datasets. Of these, ∼250 miRNAs were significantly regulated ($FC \geq 2$ and $P \leq 0.001$) in each dataset. To derive a robust list of miRNA candidates that are regulated during maturation, we only chose those miRNAs that were significantly regulated in both 1y-CM and cEHTs. This resulted in a list of 77 miRNAs (Dataset S5). Myogenic miRNAs (myomiRs) such as miR-1, miR-208, and miR-133 were significantly changed in only one of the two datasets (*SI Appendix*, Fig. S4*A*). A heat map analysis of the 77 miRNAs in the two datasets revealed four groups of miRNAs (Fig. 2*B* and *SI Appendix*, Fig. S4*B*): Some representative candidates of miRNAs up-regulated in both datasets (group 1) were members of the let-7 and mir-378 families and mir-30. Similarly, candidate members that were down-regulated in the both datasets were mir-502 and mir-129 (group 2). To delineate the pathways most significantly regulated by miRNAs during CM maturation, we analyzed two groups of miRNA–mRNA interactions from 1y-CMs using IPA and an miRNA-mRNA target filter algorithm: the overlap between the targets of down-regulated miRNAs and up-regulated mRNA in mature CMs, and the overlap between the targets of up-regulated miRNAs and down-regulated mRNAs during maturation. The three miRNAs showing the highest number of targets in our mRNA dataset were let-7, mir-378, and mir-129 (Fig. 2 *A–C*), and they thus were chosen for further pathway analysis using Genemania (www.genemania.org) and/or previous literature. Interestingly, a pathway analysis algorithm of Genemania revealed that a considerable number of the let-7 targets that were down-regulated in CM maturation belonged to PI3/AKT/insulin signaling (Dataset S6). Because the let-7 family is one of the most highly up-regulated miRNAs in both cEHTs and 1y-CMs, and because this miRNA family has the largest number of down-regulated targets in the mature CMs and a large subset of its targets belonged to the insulin signaling pathway, we chose to examine let-7 in more detail in relation to CM maturation.

**Let-7 Family Required and Sufficient for Maturation of hESC-CM.** To first test whether let-7 is required for maturation of hESC-CM, we targeted to KD all members of the let-7 family by constitutively OE Lin28a, a negative regulator of let-7, for up to 2 wk in Rockefeller University embryonic stem 2 (RUES2)-CMs. To do this, we used a lentiviral-based cloning vector, pLVX, carrying a Zs-Green reporter, and all analyses of let-7 KD were carried out when the CMs were roughly at day 30. The transduction efficiency attained by counting the number of Zs-Green-positive cells was up to 70 ± 10%. qPCR validated the lin28a expression to be 40-fold higher in Lin28a OE CMs compared with the empty vector (EV) control (Fig. 3*A*). Furthermore, we selected a member of the let-7 family, let-7g, for further qPCR validation and found that let-7g showed a significant down-regulation in Lin28a OE CMs (Fig. 3*B*). Interestingly, down-regulation of let-7 correlated with the repression of several known maturation markers in Lin28 OE CMs (Fig. 3*C*). This further encouraged us to characterize multiple parameters that have been shown to be

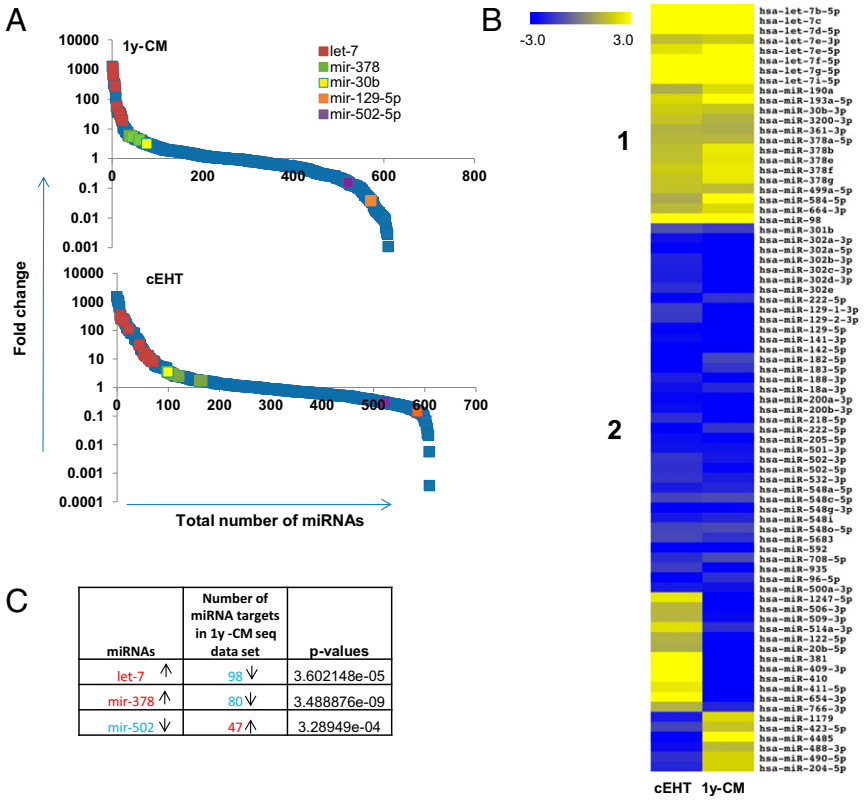


C

| miRNAs | Number of miRNA targets in 1y -CM seq data set | p-values |
|---|---|---|
| let-7 ↑ | 98 ↓ | 3.602148e-05 |
| mir-378 ↑ | 80 ↓ | 3.488876e-09 |
| mir-502 ↓ | 47 ↑ | 3.28949e-04 |

**Fig. 2.** Genome-wide sequencing of in vitro-matured CMs reveals let-7 as the most highly expressed miRNA family. (*A*) Plot depicting expression of all miRNAs with deducible read counts. The *x* axis indicates ranks of miRNAs based on relative fold change expression (*y* axis). Colored points highlight members of various miRNA families, including let-7d, let-7g, let-7f, let-7b, and let-7i; mir-378f, mir-378g, mir-378e, mir-378b, mir-378a, mir-378i, and mir-378c; mir-30b; mir-129–5p; and mir-502–5p. (*B*) Heat map generated using multiexpression viewer (mev.tm4.org) includes fold changes of all significantly regulated miRNAs (FC ≥ 2 and $P \leq 0.001$) in common between 1y-CMs and cEHTs relative to day 20-CMs. Yellow and blue indicate up- and down-regulation, respectively. Numbers: 1 and 2 indicate significantly up- or down-regulated miRNAs, respectively. (*C*) miRNA-mRNA target analysis using IPA with 1y-CM expression datasets: three miRNAs with the highest number of targets in 1y-CMs. *P* values reflect a one-sided Fisher's exact test calculated using the total number of targets for each miRNA and the number of targets present in the dataset.

modulated during cardiac developmental maturation (21). For these studies, we performed α-actinin (Z-disk protein) staining to visualize the EV control and Lin28a OE CMs ($n = 3$; >50 cells each) (Fig. 3*D*). We found a significant decrease in cell perimeter (Lin28a OE, 25 ± 3 μm vs. EV, 108 ± 13 μm; $P < 0.001$), cell area (Lin28a OE, 30 ± 17.5 $\mu m^2$ vs. EV, 400 ± 30 $\mu m^2$; $P < 0.001$), and sarcomeric length (Lin28a OE, 1.1 ± 0.09 μm vs. 1.65 ± 0.13 μm; $P < 0.001$) (Fig. 3 *E*–*G*). Conversely, circularity index [4π area/(perimeter)$^2$] increased from 0.44 ± 0.03 in EV to 0.60 ± 0.04 in Lin28a OE CMs (Fig. 3*H*). To determine whether the Lin28 OE phenotype is dependent on let-7 function, we overexpressed let-7g, using let-7g mimics in Lin28 OE CMs. Using multiple parameters, we found that let-7g OE was able to partially rescue the Lin28 OE phenotype (Fig. *A*–*H*). In addition, we also knocked down let-7g, using let-7g antagomir (Fig. 3*I*). Interestingly, KD of let-7g resulted in a phenotype similar to that seen in lin28OE CMs (Fig. 3 *J*–*N* and *SI Appendix*, Fig. S6*A*), suggesting a normal level of let-7 is required for maturation in hESC-CMs.

To further examine whether let-7 is sufficient to induce CM maturation, we selected two members of the let-7 family, let-7g and let-7i, according to their fold-change, as well as *P* values. These were further validated for their up-regulation using qPCR in cEHTs, 1y-CMs, and HAH samples in comparison with day 20-CMs (Fig. 4*A*). For further functional analyses, we used a lentiviral-based pLKO cloning system to independently overexpress these candidates for up to 2 wk in RUES2-CMs. The overall transduction efficiency of the lentivirus in the RUES2-CMs was assessed to be ∼60%, using a Ds-Red-encoding virus (*SI Appendix*, Fig. S5; $n > 25$ cells from three biological replicates). qPCR analysis validated let-7i and let-7g overexpression in CMs that were transduced with let-7 OE lentiviruses (Fig. 4*B*). In comparison with the EV control, let-7 OE CMs also exhibited a significant increase in all of the cardiac maturation markers that were previously found to be up-regulated in the cEHTs and 1y-CMs (Figs. 1*B* and 4*C*). However, let-7 OE did not change the expression of myomiRs. Similar results were obtained when let-7g OE was carried out using let-7g mimics. In this case, transient transfections were carried out in RUES2-CMs at day 15 and day 22, and end-point assays were done at day 30 (*SI Appendix*, Fig. S6 *B* and *C*). This provided the first indication that overexpression of let-7 could accelerate the maturation process. Applying the same parameters used for Lin28a OE CMs, we further characterized let-7 OE CMs. In contrast to what we observed with the Lin28a OE CMs, α-actinin (Z-disk protein) staining demonstrated a significant increase in cell perimeter (let-7i OE, 300 ± 7.4 μm; let-7g OE, 302 ± 3 μm vs. 108 ± 15 μm; $P < 0.001$), cell area (let-7i OE, 1,110 ± 101 $\mu m^2$; let-7g OE, 980 ± 95 $\mu m^2$ vs. 380 ± 70 $\mu m^2$; $P < 0.001$) (Fig. 4 *D*–*F* and *SI Appendix*, Fig. S6*D*) in let-7 OE CMs. Circularity index decreased in CMs that were overexpressing let-7i and let-7g vs. EV control (let-7i OE, 0.15 ± 0.04; let-7g OE, 0.12 ± 0.02 vs. 0.41 ± 0.02) (Fig. 4 *D* and *G*). We also found that the sarcomere length increased from 1.65 ± 0.02 μm in EV control cells to 1.70 ± 0.01 μm and 1.69 ± 0.01 ($P < 0.001$) in let-7i and let-7g OE samples, respectively (Fig. 4 *D* and *H*).

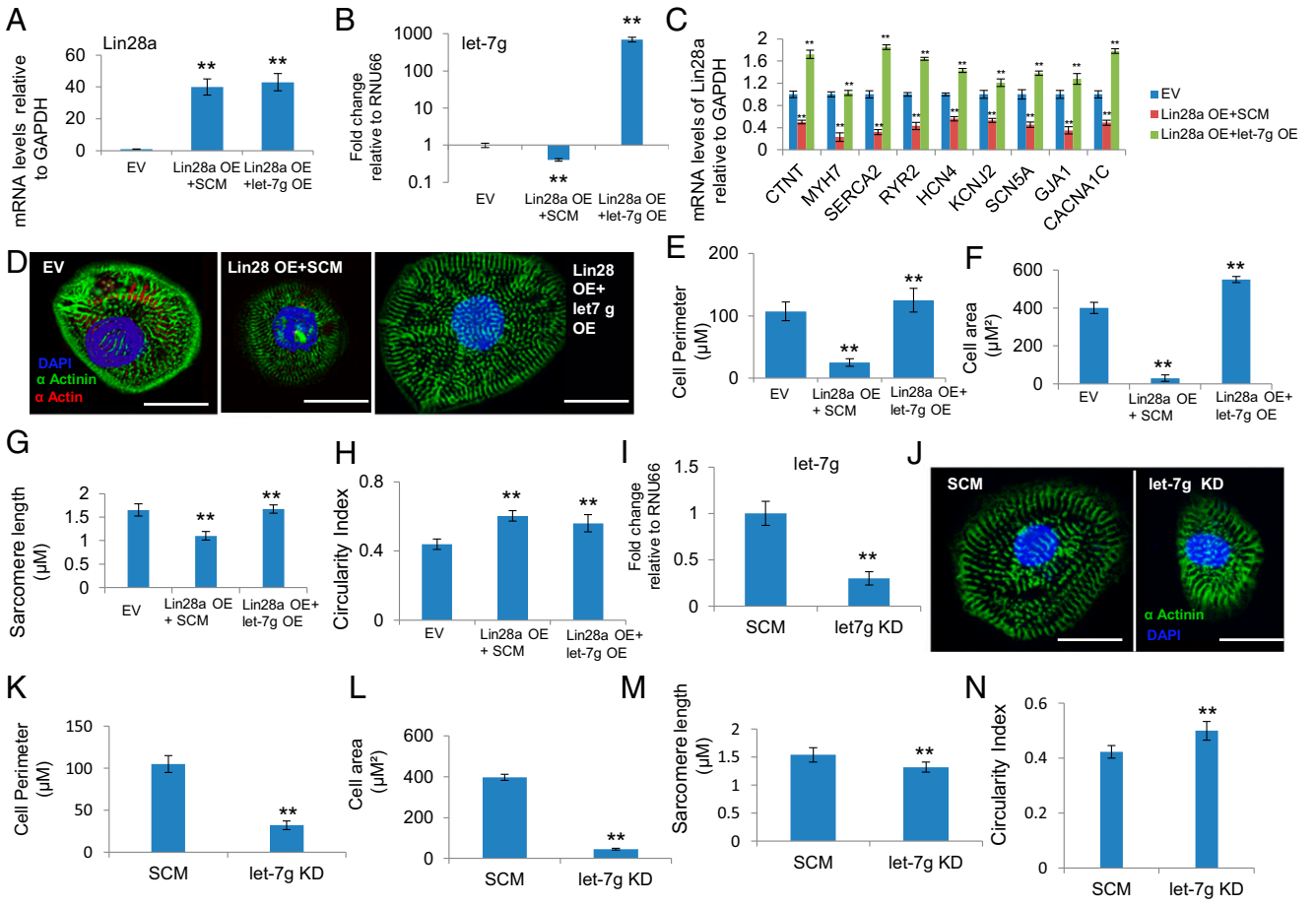


**Fig. 3.** Let-7 is required for hESC-CM maturation. (*A–K*) All analyses done in EV control, Lin28a OE, and Lin28a OE+ let-7g OE CMs. (*A–C*) qPCR analysis to (*A*) examine Lin28a expression, (*B*) demonstrate that let-7g is down-regulated in Lin28a OE CMs but its expression is rescued in response to let-7g OE using let-7g mimics, and (*C*) evaluate the expression of maturation markers. (*D*) α-Actinin (green) and DAPI (blue) staining of representative CMs from the three treatments. (Scale bar = 25 μm.) (*E–H*) Compared with EV control, Lin28a OE CMs showed significant decrease in (*E*) cell perimeter, (*F*) cell area, and (*G*) sarcomere length and (*H*) an increase in circularity index. The phenotype was partially rescued in Lin28a OE CMs+let-7g OE. (*I–N*) All analyses done in SCRAMBLE (SCM) control and let-7g antagomir-treated CMs. (*I*) qPCR analysis to examine let-7g expression. (*J*) α-Actinin (green) and DAPI (blue) staining of representative CMs from the two treatments. (Scale bar = 25 μm.) (*K–N*) Compared with SCM control, let-7g KD CMs showed significant decrease in (*K*) cell perimeter, (*L*) cell area, and (*M*) sarcomere length and an increase in (*N*) circularity index. $n = 50$ cells per condition, three biological replicates. Means ± SEM are shown. $^{**}P \leq 0.05$ (Student's *t* test). All experiments were repeated at least three times, and representative results are shown for *D* and *J*.

An increase in sarcomeric length generally corresponds to an increase in the force of contraction.

To characterize force production on a per cell basis, we used arrays of microposts to measure their contractile forces (Fig. 4*I*) (38). EV control CMs exhibited a twitch force of 7.77 ± 0.7 nN/cell. Let-7i and let-7g OE CMs exhibited a significantly higher average twitch force of 11.32 ± 0.86 and 9.28 ± 0.7 nN per cell ($P < 0.001$), respectively (Fig. 4 *I* and *J*). In addition, let-7 OE CMs (let-7i OE, 1.05 ± 0.1 hz; let-7g OE, 0.92 ± 0.094 hz) exhibited lower beat frequency compared with EV control (1.57 ± 0.1h z). This decrease in frequency corresponds well with what is seen in in vivo human heart development (i.e., as CMs mature, they begin to exhibit reduced beating frequency) (39). To examine whether let-7 supports CM maturation at an electrophysiological level, we overexpressed let-7g and let7i in transgenic RUES2-CMs stably expressing a voltage sensor protein called Arclight (40, 41). Using the Arclight sensor, we found that induction of let-7i and let-7g prolonged the action potential duration at 90% (APD90) repolarization time at room temperature (500 ± 22 ms; control, 900 ± 90 ms; $P < 0.01$) (Fig. 4 *L–N*). Moreover, let-7i OE and let-7g OE CMs displayed an increase in the ratio of action potential duration (APD50/APD90) (Fig. 4*O*), suggesting let-7 overexpression drives the CMs toward more ventricular-type CMs. Consistently, we also saw an increase in the expression of CACNA1C, an L-type Ca channel protein, suggesting there is an increase in inward depolarizing current (Fig. 4*C*) in let-7 OE CMs. The increase in APD90 and APD50/90, as well as increased expression of CACNA1C, has been shown to occur during cardiac maturation (42, 43). These data together demonstrate not only that let-7 OE results in morphological and molecular changes indicative of maturation but also that functionally relevant parameters, such as APD, contraction, and beat frequency, are appropriately regulated.

To further understand the effects of let-7 OE during CM maturation at a molecular level, we carried out whole-genome transcriptome profiling of let-7g OE CMs and corresponding EV control CMs using an Illumina RNA sequencing platform. Consistent with our qPCR data, several known maturation markers such as ryanodine receptor 2 (RYR2), myosin heavy chain 7 (MyH7), and inward rectifier potassium channel protein KCNJ2, showed increased expression in the let-7g OE CMs compared with EV control (Fig. 5*A* and *SI Appendix*, Fig. S7*A*). Using expression values for the genes that belonged to the 12 pathways (Fig. 1*E* and Dataset S2), we carried out a 2D-PCA comparing let-7g OE CMs

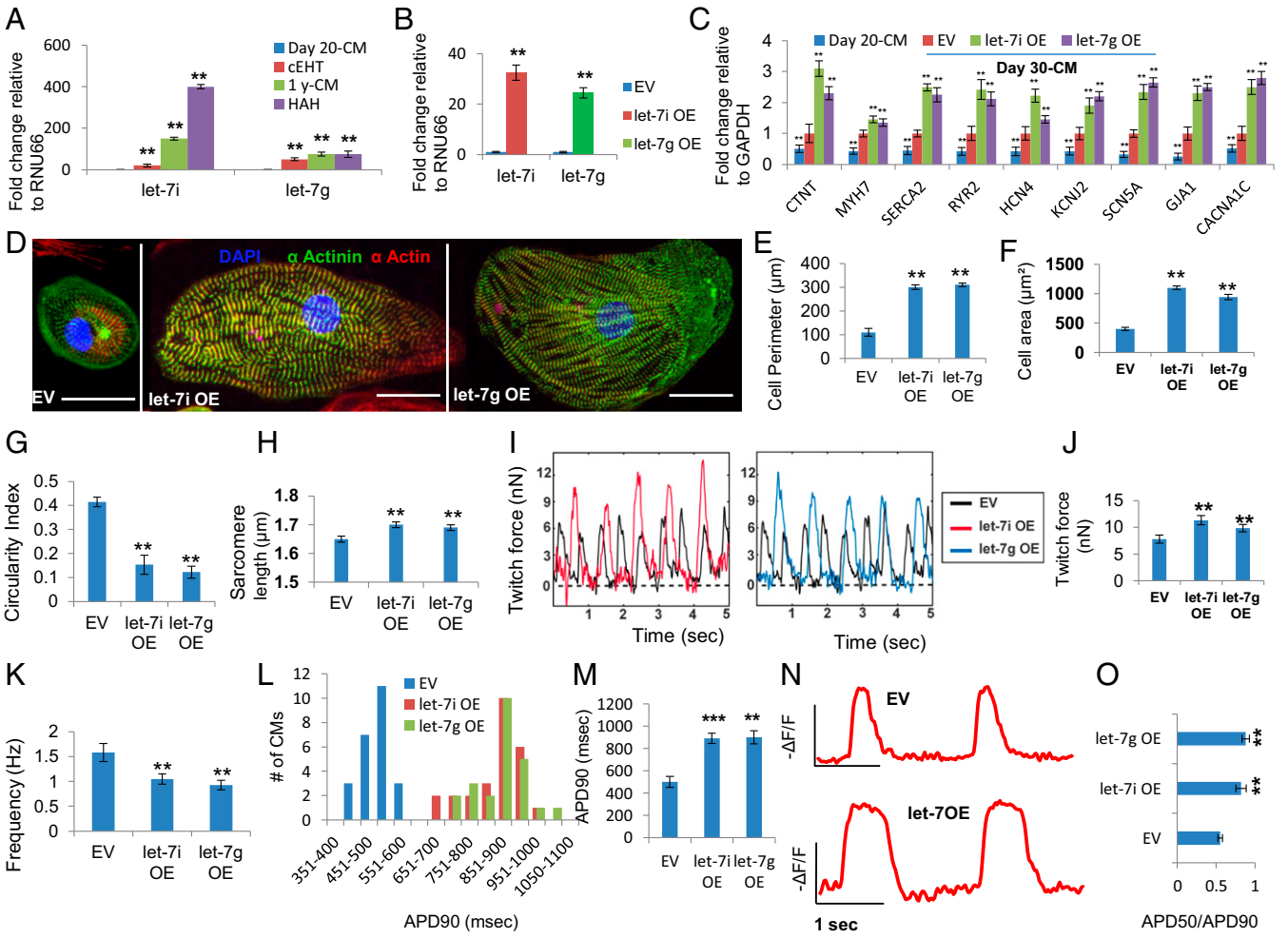


**Fig. 4.** Let-7 is sufficient for hESC-CM maturation. (*A–C*) qPCR analysis to (*A*) validate let-7i and let-7g expression derived from miRNA sequencing analysis from day 20-CM, in vitro-matured CMs, and HAH, and (*B*) demonstrate that let-7i and let-7g OE in RUES2-CMs results in increased expression of the two members. EV indicates empty vector control in RUES2-CMs (three biological replicates were analyzed for let-7 OE and EV samples). (*C*) Examine the expression of maturation markers in H7 day 20-CMs, EV, and RUES2-CMs. Gene expression is shown normalized first to GAPDH and then normalized to EV control. (*D*) α-Actinin (green), α-actin (red), and DAPI (blue) staining of representative EV control, let-7i OE, and let-7g OE CMs. (Scale bar = 50 μm.) Compared with EV control, let-7 OE CMs showed significant changes in (*E*) cell perimeter, (*F*) cell area, (*G*) circularity index, and (*H*) sarcomere length. $n = 50$ cells per condition, three biological replicates. (*I*) Representative force traces in EV control and let-7 OE CMs. (*J*) Significant increase in twitch force in let-7 OE CMs. $n = 25$ for EV control, $n = 32$ for let-7i OE, and $n = 29$ for let-7g OE from a total of three biological replicates. (*K*) Frequency of beating CMs. Compared with EV control, let-7 OE CMs show an increase in (*L–N*) APD, APD90, and (*O*) APD50/APD90. EV, let-7i OE, and let-7g OE CMs are collected at day 30 and hence are 10 d older than day 20 samples. Means ± SEM are shown. $^{**}P \leq 0.05$ and $^{***}P \leq 0.001$ (Student's *t* test). All experiments were repeated at least three times and representative images are shown for *D*.

and EV control CMs with H7-CMs at day 20 and 1y, IMR90 iPSC CMs at 1y, HAH, and 3-mo-old HFA and HFV samples. This analysis clearly separated the day 20-CMs from 1y-CMs derived from H7 and IMR90iPSCs and HAH in dimension 1 (41% variance), suggesting dimension 1 portrays the effect of maturation (Fig. 5*B* and *SI Appendix*, Fig. S7*B*). Significantly, let-7g OE was closer to 1 y than the EV and day 20 CMs in the first dimension, suggesting overexpression of let-7g does indeed accelerate maturation. Further evidence of let-7g–directed maturation was observed from known isoform changes accompanying CM maturation, such as a decrease in ratio of myosin heavy chain 6/myosin heavy chain 7 (*SI Appendix*, Fig. S8) (44, 45). Further, a new differential splicing analysis tool (*Materials and Methods*) identified 80 isoforms that show a consistent differential splicing pattern across all of the sequenced samples, selected excluding let-7 OE CMs (Datasets S7 and S8). When comparing H7-CM day 20 and the EV control with H7-CM 1 y fetal and adult samples, all but three of these isoforms were found to change monotonically, either increasing or decreasing in relative expression with maturity (Fig. 5*C*), indicating that despite the variety of tissues sequenced, cell maturation is the strongest determinant in the splicing changes we observe. We then used these isoforms as a benchmark of splicing maturity, evaluating splicing rates in let-7 OE CMs. Hierarchical clustering groups let-7 OE CMs with the 1 y and fetal samples (Fig. 5*C*), and a similar pattern is seen when principal component analysis is applied (Fig. 5*D*). In short, concerted and dynamic changes in splicing during maturation are observed in in vitro-matured and let-7 OE CM samples. Interestingly, among the 80 genes, several have been shown to be involved in cardiogenesis, including troponin T2 (TNNT2) (46) (*SI Appendix*, Fig. S9). The fact that both differential splicing and differential expression analyses cluster let-7 OE CMs with H7 1y-CM and fetal samples (Fig. 5 *B* and *D*) clearly strengthens the finding that let-7 is critical for maturation. These results demonstrate that let-7 is not only required but also sufficient for maturation of hESC-CMs.

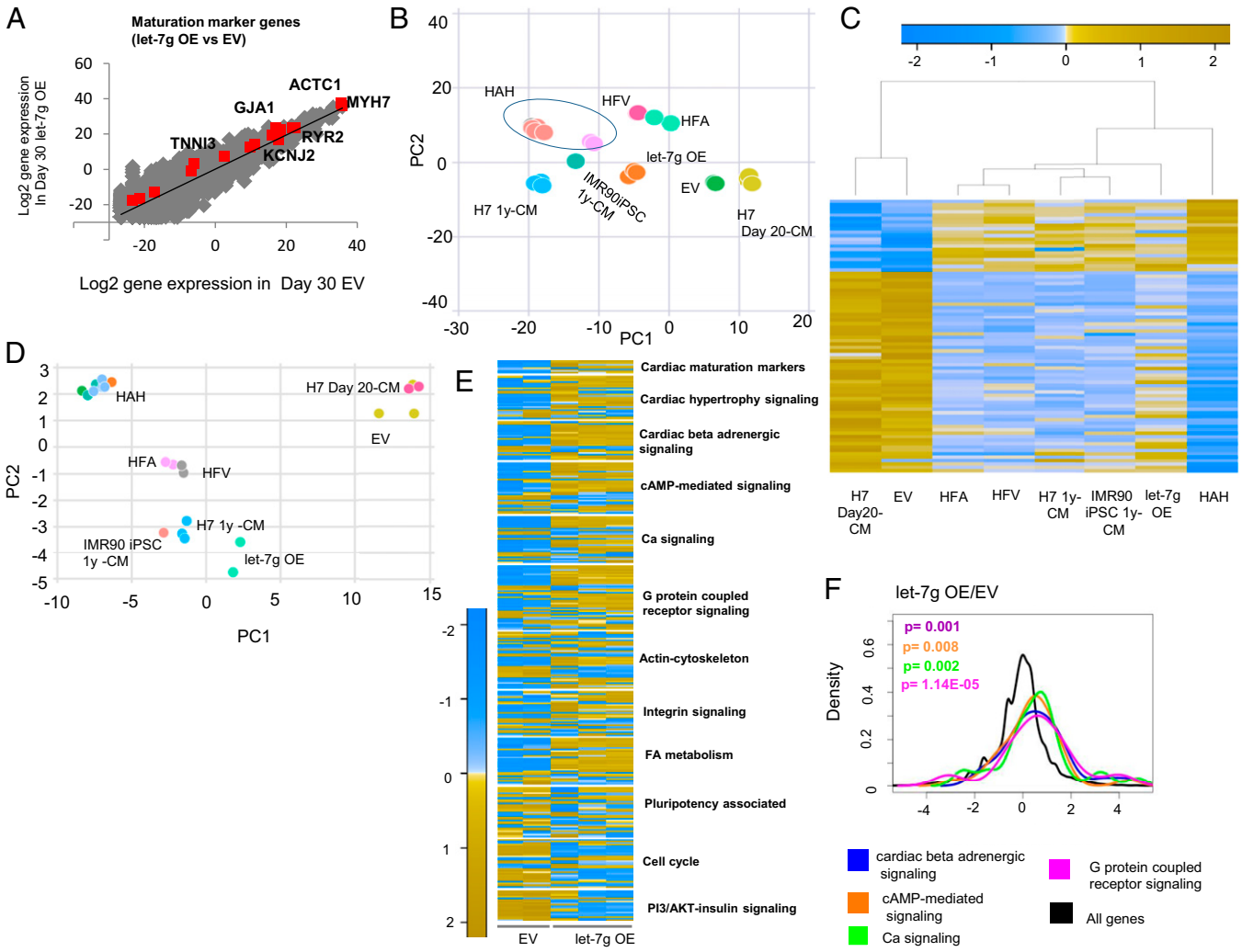


**Fig. 5.** Let-7 is critical for cardiac maturation (*A*, *B*, *E*, and *F* are analyses done with gene expression analyses and *C* and *D* are analyses based on splice variant signatures). (*A*) Scatter plot of let-7g OE (*y* axis) vs. EV control (*x* axis) from the mRNA sequencing dataset. Red dots indicate maturation marker genes in the dataset. A few are labeled in the plot: troponin I type 3 (TNNI3); gap junction protein alpha 1 (GJA1); actin alpha cardiac muscle 1 (ACTC1); myosin heavy chain 7 (MYH7); ryanodine receptor 2 (RYR2); potassium channel, subfamily J2 (KCNJ2); sodium channel protein 5 alpha (SCN5A); sarco endoplasmic reticulum $Ca^{2+}$ATPase 2 (SERCA2); troponin T type 2 (TNNT2); calcium channel, voltage dependent, alpha 1C (CACNA1C). (*B*) 2D-PCA using mRNA signatures from 12 pathways (indicated in Fig. 1*E*) across the analyzed samples, as indicated in the figure. (*C*) Heat map showing the proportion of each of the 80 isoforms identified as differentially spliced across each condition. Each value is the estimated proportion of that isoform among all expressed isoforms of the same gene in that condition. (*D*) 2D-PCA based on the proportions of the 80 identified differentially spliced transcripts, applied to all replicates from these eight conditions. (*E*) Heat map demonstrating changes in gene expression of 12 different pathways between EV control and let-7g OE CMs. Left to right, columns 1–2 and 3–5 represent biological replicates of EV and let-7g OE CMs, respectively. The rows reflect read counts of various genes in the different categories. Rows are standardized individually and colored according to the Z score. Yellow and blue represent up- and down-regulation, respectively. (*F*) Density plots using R generated with fold change expression (*x* axis indicates $\log_2$-fold change) of genes from four categories, indicative of cardiac function for let-7 OE/EV CMs. Black curve indicates expression of all genes. Curves toward the left and right side of the black curve indicate down-regulation and up-regulation of pathways, respectively.

**Let-7 Promotes hESC-CM Maturation by Acting as a Metabolic Switch.** To understand the molecular signaling components of the maturation program that are modulated in let-7g OE CMs, we further probed the transcript profiling data from let-7g OE CMs for each of the 12 pathways previously identified (Fig. 5*E*). Pathways related to Ca signaling, G protein-coupled receptor signaling, cAMP-mediated signaling, and cardiac beta adrenergic signaling and hypertrophic signaling were significantly up-regulated in let-7 OE CMs, similar to that seen in 1y-CMs and fetal heart tissue samples (Fig. 5 *E* and *F* and *SI Appendix*, Fig. S10*A*). Importantly, fatty acid metabolism was significantly up-regulated, whereas PI3/AKT/insulin signaling was significantly down-regulated in the let-7g OE CMs in comparison with EV control (Fig. 6*A*). Programs related to cell cycle, actin-cytoskeleton, and integrin signaling also showed the correct trends (*SI Appendix*, Fig. S10 *A* and *B*). The inverse relationship between fatty acid metabolism and PI3/AKT/insulin signaling in let-7g OE CMs was similar to that observed in the 1-y-old CMs and consistent with the metabolic switch seen in maturing CMs in in vivo studies. Using let-7 OE CMs, we validated by qPCR the down-regulation of candidate let-7 targets such as EZH2 and those in the insulin pathway, as well as the up-regulation of genes in fatty acid metabolism (Fig. 6*B*).

To test the functional relevance for these gene expression changes, we carried out metabolic analysis of let-7 OE CMs vs. EV control, using the Sea Horse metabolic flux assay. First, we analyzed mitochondrial maximal respiration capacity by measuring the oxygen consumption rate (OCR), a metabolic pa-

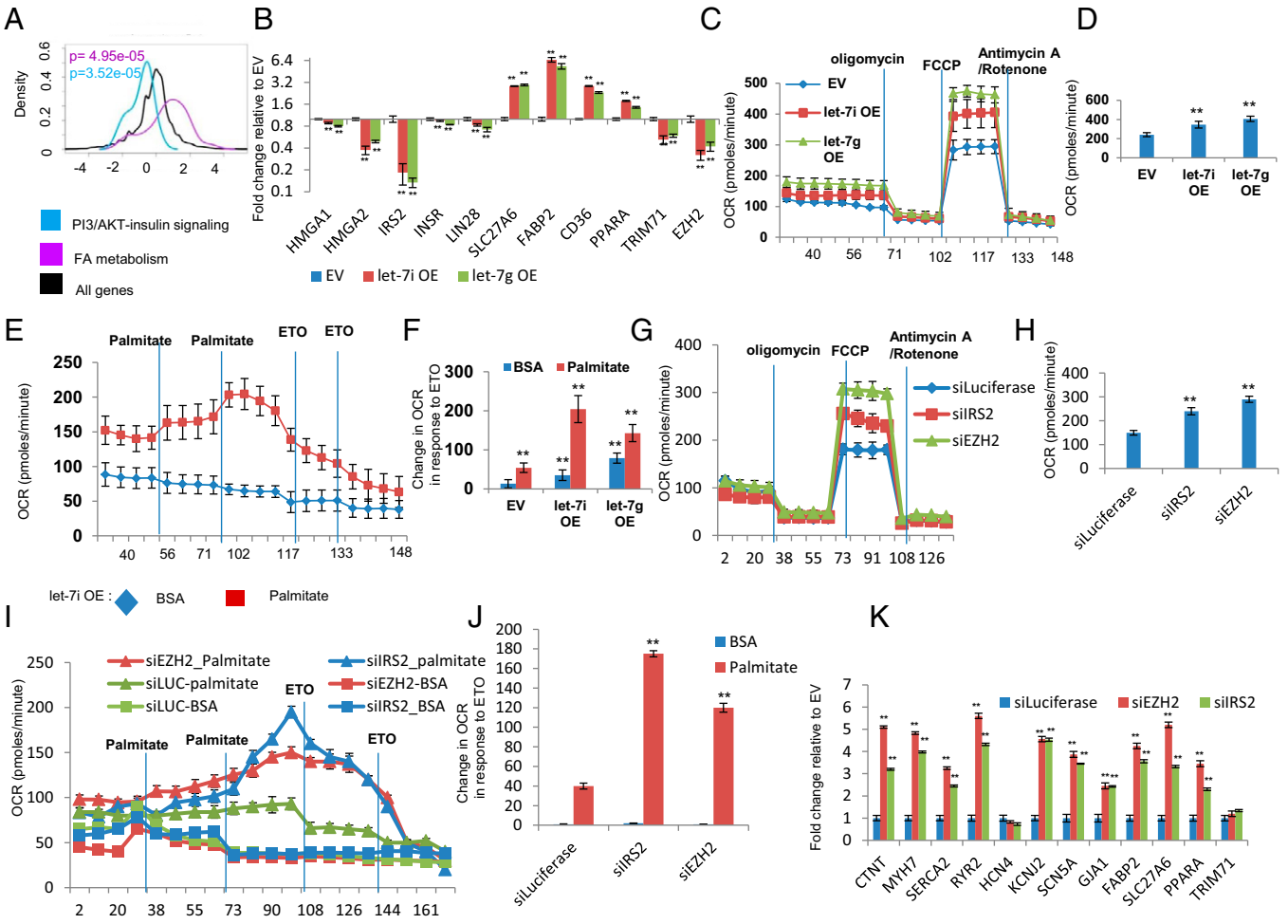


**Fig. 6.** Let-7 OE accelerates CM maturation. (*A–F*) Let-7 OE results in down-regulation of the PI3/AKT/Insulin pathway and up-regulation of fatty acid metabolism. Comparisons were done between let-7 OE and EV control for all assays. (*A*) Density plots using R generated with fold change expression (let-7g OE/EV) of genes for fatty acid metabolism and PI3/AKT/insulin signaling. (*B*) qPCR analysis of candidate let-7 targets and genes from the fatty acid metabolism. (*C*) Representative OCR profile in response to ATP synthase inhibitor oligomycin, uncoupler of electron transport and oxidative phosphorylation, FCCP, and electron transport chain blockers rotenone and antimycin during mito-stress assay. (*D*) Quantification of maximal respiration capacity; that is, changes in response to FCCP treatment after inhibition of ATP synthase by oligomycin. $n = 24$ from three biological replicates. (*E*) Representative OCR trace of let-7g OE CMs for fatty acid stress measuring Etomoxir (ETO)-responsive OCR changes after the second dose of palmitate addition. (*F*) Quantification of changes in OCR in response to ETO. $n = 32$ from three biological replicates. Means ± SEM are shown. $^{**}P \leq 0.05$ (Student's *t* test). (*G–K*) Knock-down of IRS2 and EZH2 results in up-regulation of fatty acid metabolism and improved expression of cardiac maturation markers. (*G* and *H*) Representative OCR profile and quantification of maximal respiratory capacity in siIRS2-CM and siEZH2-CM. (*I* and *J*) Representative OCR trace for fatty acid stress using palmitate and quantification of OCR change (*E*). (*K*) qPCR analysis of cardiac maturation markers, fatty acid metabolism genes.

rameter representing mitochondrial respiration levels. To record the maximum activity of the electron transport chain uncoupled from ATP synthesis, mitochondrial ATP synthase was inhibited with oligomycin, and then maximum mitochondrial respiration was measured after addition of the proton gradient discharger, carbonyl cyanide 4-(trifluoromethoxy)phenylhydrazone (FCCP). The OCR changes were significantly greater after FCCP treatment in let-7i OE and let-7g OE CMs compared with in EV control samples (Fig. 6 *C* and *D*). Increased mitochondrial respiration could be a result of increased mitochondrial copy number or increased mitochondrial activity; for example, as a result of higher efficiency of glucose or fatty acid use as energy substrates. We determined mitochondrial genome copy number by qPCR and found that let-7 OE had no effect on this parameter (*SI Appendix*, Fig. S11*A*). Interestingly, fatty acid stress test using palmitate revealed that the let-7g OE and let-7i OE CMs have greater OCR increase in response to palmitate than EV control (Fig. 6 *E* and *F*). To investigate whether the let-7 OE CMs also use glucose more efficiently, the extracellular acidification rate was determined. No significant difference was observed in the maximum extracellular acidification rate changes in the glucose stress assay for let-7 OE compared with for EV control (*SI Appendix*, Fig. S11 *B* and *C*). Together, these data indicate that the let-7 family of miRNA likely induces hESC-CM maturation in part by promoting a higher use of fatty acids to meet the CM's increased energy demands. To further dissect the mechanism of let-7 function in this process, we chose to KD two validated targets of let-7: IRS2, a member of an insulin signaling pathway, and EZH2, a histone methyl transferase known to regulate gene expression (47). These two candidates were found to be down-regulated in let-7g OE CMs (Fig. 6*B*). Interestingly, siRNA KD of IRS2 and EZH2 in RUES2 CMs (*SI Appendix*, Fig. S11*D*) resulted in an increase in OCR (Fig. 6 *G* and *H*), as well as a higher efficiency in the use of palmitate (Fig. 6 *I* and *J*), compared with their siLuciferase control. Moreover, KD of IRS2 and EZH2 resulted in an increased expression of cardiac maturation genes as well as genes from fatty acid metabolism (Fig. 6*K*). However, E3 ubiquitin-protein ligase TRIM71, a target of let-7, did not show any change

in expression in both siIRS2 and siEZH2 CMs (Fig. 6*K*). These data suggest that let-7 exerts its function on cardiac maturation in part by simultaneously acting on two of its targets, IRS2 and EZH2.

**Let-7g Exclusively Promotes in Vitro Cardiac Maturation, and Not Early Cardiac Commitment.** Previous reports have demonstrated that induction of let-7 silences ESC self-renewal, or inhibition of let-7 promotes dedifferentiation of fibroblasts to a pluripotent state, showing that let-7 inhibits a stem cell state and suggests let-7 could have a role in early lineage commitment (48). Similarly, using in vivo mouse studies, Colas et al. (49) have shown that let-7 can promote mesodermal commitment during embryonic development. However, none of these studies have specifically demonstrated the role of let-7 in early cardiac commitment. To address this, we first carried out an elaborate time course expression analysis of let-7g, a candidate member of the let-7 family (*SI Appendix*, Fig. S12 *A* and *B*). We found that the expression of let-7g is very minimal at stages of mesodermal commitment (days 2–3), as well as commitment to cardiac lineages (day 5). However, a dramatic increase is observed during later points in our in vitro cardiac differentiation system (day 20–1 y). To gain more insights on this, we overexpressed let-7g using let-7g mimics at day 5 of the differentiation, where previous report has shown that cardiac commitment occurs (50). After 3 d of early let-7g OE, we monitored the expression of three known early cardiac markers [myosin light chain 2 (MLC2), basic helix-loop-helix family of transcription factor HAND2, zinc-finger family of transcription factor GATA4], whose expression was found to increase at early points (51). Interestingly, overexpression of let-7g, even as high as 1,000-fold (*SI Appendix*, Fig. S12*C*), and down-regulation of some of its targets (*SI Appendix*, Fig. S12*D*) did not change the expression of these cardiac markers after 3 d (*SI Appendix*, Fig. S12*E*). These data altogether demonstrate that the function of let-7g is rather exclusive during cardiac maturation.

## Discussion

In this study, for the first time to our knowledge, we demonstrate that the let-7 family of miRNAs is required and sufficient for maturation of hESC-CMs. A wide range of functional, physiological, electrophysiological, and molecular parameters indicates that induction of candidate members of the let-7 family is sufficient to enhance a number of functional properties relevant to CM maturation. In contrast, KD of let-7 either by Lin28 OE or using antagomir for let-7g results in attenuating the process. Interestingly, introduction of let-7g mimics partially rescues the Lin28 OE phenotype in CMs, suggesting let-7 acts independently of Lin28 in the cardiac maturation pathway. Previous genetic studies have shown that the shift in cardiac fuel preference from glucose to fatty acids taking place during fetal to postnatal transition (3) is largely mediated by the PPARα-PPARγ coactivator-1α axis (52). However, our study has identified a previously unsuspected regulator that could promote this metabolic transition in sync with cardiac maturation. Overexpression of let-7g and let-7i specifically accelerates the CM's capacity to use fatty acid as a major energy source without affecting mitochondrial copy number or improving the efficiency of glycolysis. Because these metabolic and functional changes mimic changes during postnatal maturation, we posit that induction of let-7 in young CMs results in changes that are equivalent to physiological hypertrophy (3). Thus, in addition to studies that have proposed using let-7 as a therapeutic tool for attenuating myocardial infarction (53), we propose that this miRNA can be potentially used for improving cardiac function during maturation.

Maturation of CMs is complex and bound to be regulated by multiple pathways acting simultaneously. In this context, let-7 is a great candidate, as it regulates a multitude of target genes that could potentially promote maturation. A direct inhibition of two such let-7 targets, IRS2 and EZH2, phenocopied let-7 OE on cardiac maturation, suggesting let-7 imparts its metabolic effect on CM maturation by acting on at least two of its targets. EZH2 is a histone methyltransferase and component of polycomb repressive complex, which methylates H3K27, resulting in the transcriptional repression of affected targeted genes (47). One attractive hypothesis is that EZH2 either directly or indirectly represses genes involved in fatty acid oxidation, and let-7-driven down-regulation of EZH2 releases transcriptional repression of fatty acid oxidation genes. Consistent with this hypothesis, repressing EZH2 resulted in an increased expression of candidate fatty acid genes. However, further experiments are needed to elucidate the interplay of IRS2, EZH2, and other key let-7 targets in cardiac maturation in greater detail. The fact that TRIM71, another candidate let-7 target, remains unchanged in siIRS2-CM and siEZH2-CM, but is significantly repressed in let-7 OE CMs, clearly suggests the multipronged function of let-7 as a developmental switch (*SI Appendix*, Fig. S13). Because let-7 is found to be highly expressed in other cell types such as late retinal progenitors and glial cells (54, 55), further studies to address the mechanism by which let-7 regulates cardiac maturation would also shed light on maturation of other cells types in vitro. In conclusion, our discovery of a small RNA essential to promote cardiac maturation and metabolic transition provides a unique focus for the rational development of strategies for generating mature tissue types useful for regenerative medicine.

## Experimental Procedures

**Cell Culture.** Undifferentiated hESC lines H7 (NIHhESCC-10-0061) and RUES2 (NIHhESC-09-0013) were expanded using mouse embryonic fibroblast-conditioned medium and subjected to directed differentiation under serum- and insulin-free conditions.

**Immunocytochemistry and Morphological Analysis.** Cells were fixed in 4% (vol/vol) paraformaldehyde, blocked for an hour with 1.5% (vol/vol) normal goat serum, and incubated overnight with mouse alpha actinin (sigma clone EA-53) primary antibody, followed by secondary antibody [(Alexa fluor 488 (Goat anti mouse)] staining. Measurements of CM area, perimeter, and sarcomere length were performed using NIH Image J 1.44 software (rsb.info.nih.gov/nih-image/).

**mRNA and miRNA Sequencing Analysis.** RNA and small RNA libraries were prepared independently, using Truseq library preparation kits (Illumina), following the manufacturer's protocols. Sequence data for miRNAs were analyzed using miRDeep2 software. Both principle component analysis and hierarchical clustering were performed using log-transformed Transcript per million gene expression estimates, using R 3.0.2. Heat maps for the RNA and miRNA sequencing data were generated using the edgeR version 3.2.4 and multiexperiment viewer (www.tm4.org), respectively.

**Splice Variant Analysis.** To define a set of differentially spliced genes, we looked for changes in isoform proportions, defined as an isoform's expression divided by the sum of the expression of all isoforms with the same transcription start site. To call differential splicing, we looked for isoforms that showed a specific and consistent ordering of the immature (day 20 and EV CM) versus the mature (fetal, 1 y, and adult) samples with posterior probability >0.75. Of all but three of the 80 isoforms called, this manifested as a consistent increase or decrease between immature and mature. To increase the chances of detecting changes in splicing dynamics, the AceView gene annotations were used, which more liberally include alternate isoforms (56).

**Contractile Force Measurement.** Muscle twitches from individual hESCs-CMs were recorded with high-speed video microscopy within a live cell chamber at 37 °C, as described by Rodriguez et al. (38).

Detailed information on cell culture, lentiviral transduction, immunohistochemistry, flow cytometry, Arclight reporter analysis, qPCR and sequencing analysis, force contraction assay, and mitochondrial functional assay are provided in the *SI Appendix*.

**ACKNOWLEDGMENTS.** We thank members of the H.R.-B. laboratory, Carol Ware, Thomas Reh, and Anna La Torre, for helpful discussions; Jason Miklas and Mark Saiget for technical assistance; Savannah Cook, Benjamin van Biber, James Fugate, and Nathan Palpant for providing CMs; Thomas Reh and Deepak Lamba for gifting the lin28a OE construct; Hans Reinecke for providing HFA and HFV RNA samples; Vincent Pieribone for gifting the

Arclight Addgene plasmid #36857; Kristen Bemis for assisting in RNA sequencing; Vivian Oehler for help with IPA; and Ron Phillips for assistance in confocal microscopy. This work was supported in part by NIH Grant 3R01GM083867-03S1 and a Teitze young scientist award (to K.T.K.); National Science Foundation (NSF) graduate research fellowship (to M.L.R.); NIH Grants P01GM081619 (to H.R.-B., C.E.M., and W.L.R.), R01GM097372, R01GM083867, R01GM083867-02S2 (to H.R.-B.), P01HL094374 (to C.E.M. and M.A.L.), R01HL117991 (to M.A.L.), R01HL084642, U01HL100405 (to C.E.M.), T32HG00035 (to D.C.J.), and a NSF CAREER award (to N.J.S.), as well as support from the University of Washington Institute for Stem Cell and Regenerative Medicine (to H.R.-B. and C.E.M.) and a gift from the Hahn family to (H.R.-B.).

1. Kim C, et al. (2013) Studying arrhythmogenic right ventricular dysplasia with patient-specific iPSCs. *Nature* 494(7435):105–110.
2. Ahmad F, Seidman JG, Seidman CE (2005) The genetic basis for cardiac remodeling. *Annu Rev Genomics Hum Genet* 6:185–216.
3. Lopaschuk GD, Jaswal JS (2010) Energy metabolic phenotype of the cardiomyocyte during development, differentiation, and postnatal maturation. *J Cardiovasc Pharmacol* 56(2):130–140.
4. Chung S, Arrell DK, Faustino RS, Terzic A, Dzeja PP (2010) Glycolytic network restructuring integral to the energetics of embryonic stem cell cardiac differentiation. *J Mol Cell Cardiol* 48(4):725–734.
5. Chung S, et al. (2007) Mitochondrial oxidative metabolism is required for the cardiac differentiation of stem cells. *Nat Clin Pract Cardiovasc Med* 4(Suppl 1):S60–S67.
6. Kolwicz SC, Jr, Purohit S, Tian R (2013) Cardiac metabolism and its interactions with contraction, growth, and survival of cardiomyocytes. *Circ Res* 113(5):603–616.
7. Alaynick WA, et al. (2007) ERRgamma directs and maintains the transition to oxidative metabolism in the postnatal heart. *Cell Metab* 6(1):13–24.
8. Lehman JJ, et al. (2000) Peroxisome proliferator-activated receptor gamma coactivator-1 promotes cardiac mitochondrial biogenesis. *J Clin Invest* 106(7):847–856.
9. Lopaschuk GD, Ussher JR, Folmes CD, Jaswal JS, Stanley WC (2010) Myocardial fatty acid metabolism in health and disease. *Physiol Rev* 90(1):207–258.
10. Chen H, VanBuren V (2014) A provisional gene regulatory atlas for mouse heart development. *PLoS ONE* 9(1):e83364.
11. Olson EN (2006) Gene regulatory networks in the evolution and development of the heart. *Science* 313(5795):1922–1927.
12. Huss JM, Kelly DP (2004) Nuclear receptor signaling and cardiac energetics. *Circ Res* 95(6):568–578.
13. Kuppusamy KT, Sperber H, Ruohola-Baker H (2013) MicroRNA regulation and role in stem cell maintenance, cardiac differentiation and hypertrophy. *Curr Mol Med* 13(5):757–764.
14. Espinoza-Lewis RA, Wang DZ (2012) MicroRNAs in heart development. *Curr Top Dev Biol* 100:279–317.
15. Wilson KD, et al. (2010) Dynamic microRNA expression programs during cardiac differentiation of human embryonic stem cells: Role for miR-499. *Circ Cardiovasc Genet* 3(5):426–435.
16. Gan L, Schwengberg S, Denecke B (2011) MicroRNA profiling during cardiomyocyte-specific differentiation of murine embryonic stem cells based on two different miRNA array platforms. *PLoS ONE* 6(10):e25809.
17. Cao F, et al. (2008) Transcriptional and functional profiling of human embryonic stem cell-derived cardiomyocytes. *PLoS ONE* 3(10):e3474.
18. Davis RP, van den Berg CW, Casini S, Braam SR, Mummery CL (2011) Pluripotent stem cell models of cardiac disease and their implication for drug discovery and development. *Trends Mol Med* 17(9):475–484.
19. Lundy SD, Zhu WZ, Regnier M, Laflamme MA (2013) Structural and functional maturation of cardiomyocytes derived from human pluripotent stem cells. *Stem Cells Dev* 22(14):1991–2002.
20. Robertson C, Tran DD, George SC (2013) Concise review: Maturation phases of human pluripotent stem cell-derived cardiomyocytes. *Stem Cells* 31(5):829–837.
21. Yang X, Pabon L, Murry CE (2014) Engineering adolescence: Maturation of human pluripotent stem cell-derived cardiomyocytes. *Circ Res* 114(3):511–523.
22. Zhu H, et al.; DIAGRAM Consortium; MAGIC Investigators (2011) The Lin28/let-7 axis regulates glucose metabolism. *Cell* 147(1):81–94.
23. Frost RJ, Olson EN (2011) Control of glucose homeostasis and insulin sensitivity by the Let-7 family of microRNAs. *Proc Natl Acad Sci USA* 108(52):21075–21080.
24. Tulloch NL, et al. (2011) Growth of engineered human myocardium with mechanical loading and vascular coculture. *Circ Res* 109(1):47–59.
25. Kamakura T, et al. (2013) Ultrastructural maturation of human-induced pluripotent stem cell-derived cardiomyocytes in a long-term culture. *Circ J* 77(5):1307–1314.
26. Chong JJ, et al. (2013) Progenitor cells identified by PDGFR-alpha expression in the developing and diseased human heart. *Stem Cells Dev* 22(13):1932–1943.
27. Fearnley CJ, Roderick HL, Bootman MD (2011) Calcium signaling in cardiac myocytes. *Cold Spring Harb Perspect Biol* 3(11):a004242.
28. van der Vusse GJ, van Bilsen M, Glatz JF (2000) Cardiac fatty acid uptake and transport in health and disease. *Cardiovasc Res* 45(2):279–293.
29. Bird SD, et al. (2003) The human adult cardiomyocyte phenotype. *Cardiovasc Res* 58(2):423–434.
30. DeBosch BJ, Muslin AJ (2008) Insulin signaling pathways and cardiac growth. *J Mol Cell Cardiol* 44(5):855–864.
31. Ahuja P, Sdek P, MacLellan WR (2007) Cardiac myocyte cell cycle control in development, disease, and regeneration. *Physiol Rev* 87(2):521–544.
32. Brodsky VYa, Chernyaev AL, Vasilyeva IA (1991) Variability of the cardiomyocyte ploidy in normal human hearts. *Virchows Arch B Cell Pathol Incl Mol Pathol* 61(4):289–294.
33. Olivetti G, et al. (1996) Aging, cardiac hypertrophy and ischemic cardiomyopathy do not affect the proportion of mononucleated and multinucleated myocytes in the human heart. *J Mol Cell Cardiol* 28(7):1463–1477.
34. Lopaschuk GD, Spafford MA, Marsh DR (1991) Glycolysis is predominant source of myocardial ATP production immediately after birth. *Am J Physiol* 261(6 Pt 2):H1698–H1705.
35. Lopaschuk GD, Spafford MA (1990) Energy substrate utilization by isolated working hearts from newborn rabbits. *Am J Physiol* 258(5 Pt 2):H1274–H1280.
36. Pohjoismäki JL, et al. (2013) Postnatal cardiomyocyte growth and mitochondrial reorganization cause multiple changes in the proteome of human cardiomyocytes. *Mol Biosyst* 9(6):1210–1219.
37. Yatscoff MA, et al. (2008) Myocardial hypertrophy and the maturation of fatty acid oxidation in the newborn human heart. *Pediatr Res* 64(6):643–647.
38. Rodriguez ML, et al. (2014) Measuring the contractile forces of human induced pluripotent stem cell-derived cardiomyocytes with arrays of microposts. *J Biomech Eng* 136(5):051005.
39. Kliegman Stanton, RM BF, NF Schor, Geme JW, Behrman RE eds (2011) *Nelson Textbook of Pediatrics* (Saunders, Philadelphia, PA), pp 1529–1536.
40. Leyton-Mange JS, et al. (2014) Rapid cellular phenotyping of human pluripotent stem cell-derived cardiomyocytes using a genetically encoded fluorescent voltage sensor. *Stem Cell Rev* 2(2):163–170.
41. Jin L, et al. (2012) Single action potentials and subthreshold electrical events imaged in neurons with a fluorescent protein voltage probe. *Neuron* 75(5):779–785.
42. Sartiani L, et al. (2007) Developmental changes in cardiomyocytes differentiated from human embryonic stem cells: A molecular and electrophysiological approach. *Stem Cells* 25(5):1136–1144.
43. Ribeiro MC, et al. (2015) Functional maturation of human pluripotent stem cell derived cardiomyocytes in vitro - Correlation between contraction force and electrophysiology. *Biomaterials* 51:138–150.
44. Xu XQ, Soo SY, Sun W, Zweigerdt R (2009) Global expression profile of highly enriched cardiomyocytes derived from human embryonic stem cells. *Stem Cells* 27(9):2163–2174.
45. Mahdavi V, Lompre AM, Chambers AP, Nadal-Ginard B (1984) Cardiac myosin heavy chain isozymic transitions during development and under pathological conditions are regulated at the level of mRNA availability. *Eur Heart J* 5 Suppl F:181–191.
46. Gomes AV, et al. (2004) Cardiac troponin T isoforms affect the Ca(2+) sensitivity of force development in the presence of slow skeletal troponin I: Insights into the role of troponin T isoforms in the fetal heart. *J Biol Chem* 279(48):49579–49587.
47. Viré E, et al. (2006) The Polycomb group protein EZH2 directly controls DNA methylation. *Nature* 439(7078):871–874.
48. Peter ME (2009) Let-7 and miR-200 microRNAs: Guardians against pluripotency and cancer progression. *Cell Cycle* 8(6):843–852.
49. Colas AR, et al. (2012) Whole-genome microRNA screening identifies let-7 and mir-18 as regulators of germ layer formation during early embryogenesis. *Genes Dev* 26(23):2567–2579.
50. Paige SL, et al. (2012) A temporal chromatin signature in human embryonic stem cells identifies regulators of cardiac development. *Cell* 151(1):221–232.
51. Dubois CN, Craft AM, Sharma P, Elliott DA, Stanley EG, Elfanty AG, Gramalini A, Keller G (2011) SIRPA is a specific cell-surface marker for isolating cardiomyocytes derived from human pluripotent stem cells. *Nature Biotechnology* 29(11):1011–1019.
52. Duncan JG, Finck BN (2008) The PPARalpha-PGC-1alpha Axis Controls Cardiac Energy Metabolism in Healthy and Diseased Myocardium. *PPAR Res* 2008:253817.
53. Tolonen AM, et al. (2014) Inhibition of Let-7 microRNA attenuates myocardial remodeling and improves cardiac function postinfarction in mice. *Pharmacol Res Perspect* 2(4):e00056.
54. La Torre A, Georgi S, Reh TA (2013) Conserved microRNA pathway regulates developmental timing of retinal neurogenesis. *Proc Natl Acad Sci USA* 110(26):E2362–E2370.
55. Patterson M, et al. (2014) let-7 miRNAs can act through notch to regulate human gliogenesis. *Stem Cell Reports* 3(5):758–773.
56. Thierry-Mieg D, Thierry-Mieg J (2006) AceView: A comprehensive cDNA-supported gene and transcripts annotation. *Genome Biol* 7 Suppl 1:S12.1–S12.14.

**Supplementary Information**

## Experimental procedures

### Cell Culture

Undifferentiated human embryonic stem cell (hESCs) lines H7 (NIHhESCC-10-0061) and RUES2 (NIHhESC-09-0013) were expanded using mouse embryonic fibroblast-conditioned medium with 5ng/ml basic fibroblast growth factor. H7-CMs were derived using previously reported protocols (1-3). RUES2-CMs were used for all functional analyses and these were derived using a cardiac progenitor cell differentiation protocol derived from previously reported monolayer directed differentiation methods(1, 4, 5). In brief, this involves the induction of a monolayer of hESCs with activin A and bone morphogenetic protein-4 (BMP4) under serum- and insulin-free conditions. During the early stages of differentiation, the cells were also exposed to the Wnt agonist CHIR 99021 followed by the Wnt antagonist Xav939. From 7 days of *in -vitro* differentiation, the cells were fed every alternate day with serum-free RPMI-B27 plus insulin media. After 20 days of *in-vitro* differentiation, the cells were trypsinized and replated. Only those cell preparations that had at least 70% cardiac troponin T- positive CMs (as observed by flow cytometry) were used for further experiments. For experiments where the H7-CMs were cultured for around a year, the cells were replated after the 3$^{rd}$and 11$^{th}$ month from day 0. At the 11$^{th}$ month, FACS analysis for cTnT was conducted and the CMs were split into three parts and were cultured as three independent replicates for another 1.5 months after which they were harvested for RNA extraction. IMR90iPSC-CMs cultured for 1yr were replated at day 20 and split every 2 months for 12 months before harvesting for RNA extraction. To generate engineered cardiac tissue, we used the procedure reported by Tulloch et al.. In brief, day 20 CMs are suspended in the collagen gel at 10,000/µl, and rod-shaped constructs of 25 µl (1 mm radius x 8 mm length) were generated by casting in a preformed mold and warming to 37°C. The ends of the mold contain Velcro-like micro-fiber loops, and these become impregnated with gel + cell mixture. These tabs allow the constructs to be maintained under static tension, which facilitates

alignment and differentiation of the CMs. The constructs were maintained in the serum-free RPMI-B27 plus glutamine media up to 2 weeks. For let-7 overexpression analysis, the CMs were transduced with the virus carrying the pLKO-let-7 or empty vector control pLKO plasmid at day 12 of the directed differentiation protocol. We used the “spin method” for viral transduction where virus was added to wells carrying cardiomyocytes and spun for 1hr in a Sorvall centrifuge at 3000RPM and at 37°C followed by overnight incubation at 37°C. After overnight transduction the virus was removed, cells were rinsed with PBS and new media added. The cells were re-plated by day 17 and were analyzed at day 30 from the initiation of differentiation.

**Lentiviral transduction on cardiomyocytes**

For lenti-let7 OE constructs, Pri-miR-let7i and pri-miR-let7g sequence was amplified from H7 genomic DNA using forward primer for let7i- TCCGCGTGGTCCCGT; reverse primer for let7i-ATTGTCCTCCGCGGCGC and forward primer for let7g-AGAGTTCCTCCAGCGCTCC; reverse primer for let7g-CCCCACTTGGCAGCTGGC, resulting in 153bp and 154bp products, respectively. The amplicons were cloned between AgeI and EcoRI sites of pLKO.1 TRC vector (Open Biosystems) under human U6 promoter. 293FT cells were plated one day before transfection and pLKO.1-pri-mir-let7 was co-transfected with packaging vectors (pMK-VSVG, pMDL-G/P-RRE and pRSV-REV) in the presence of 2.5M CaCl2. Medium was changed 24 hours later and the lentiviruses were harvested 48 hours after transfection. Viral transduction of CMs was performed by a spin infection technique. In brief diluted virus in the presence of hexadimethrine bromide (Polybrene, 4µg/ml)) was added to the beating CMs at day 12 of the directed differentiation protocol. These were then subjected to centrifugation at 3000 RPM for 1 hour followed by overnight incubation with the virus.

**Transfection**

SiRNAs of IRS2, EZH2 (Ambion), let-7 mimics (Thermo Dharmacon) were transfected with Lipofectamine RNAiMAX (Invitrogen) at a 50nM concentration for each well of a 24 well plate as directed by the manufacturer. let-7 antagomirs (Thermo Dharmacon) were transfected using Dharmafect (Thermo Dharmacon) at a 100nM concentration for each well of a 24 well plate as directed by the manufacturer. Let-7 mimics and antagomirs were transfected at day 15 of the CM differentiation protocol and examined at day 30. SiRNA transfections were done at day 20 and the cells were analyzed three days later.

**Immunocytochemistry and morphological analysis**

All morphological analyses on hESC-CMs were carried out using at least 50 cells. Cells replated in chamber slides were fixed in 4% paraformaldehyde for 15 minutes followed by PBS wash. The fixed cells were blocked for an hour with 1.5% normal goat serum and incubated O/N with mouse alpha actinin (sigma clone EA-53) primary antibody. The primary antibody was rinsed with PBS and incubated with secondary antibody (Alexa fluor 488 [Goat anti mouse]) for an hour followed by nuclear staining using DAPI. For cell area and perimeter measurements, images were acquired and processed using Zeiss AXIO fluorescent microscope and Axiovision software. To attain a representative image as shown in Fig.3D and 4D, we analyzed up to 100 cells from 3 biological replicates. For sarcomere length, images were acquired and processed using Leica TCS-SPE confocal microscope and Leica software. These confocal images were used to select 1-2 myofibrils per cell with at least ten continuous, well-recognized alpha-actinin bands and divided the length value by the number of sarcomeres. The images were further analyzed using Image J software. Primary monoclonal anti-DsRed antibody (Clontech; 632393) was used at 1:200 PBT. Secondary anti-rabbit antibody was used at 1:100 PBT (Alexa Fluor 660; Invitrogen) and fish were mounted with vectashield. Images were obtained by a Nikon SMZ1500 microscope using a Nikon Digital Sight DS-Ri1 camera or confocal microscopy. Measurements of heart and cardiomyocyte size were performed using NIH Image J 1.44 software (http://rsb.info.nih.gov/nih-image/).

**Flow Cytometry**

Cardiomyocytes were fixed in 4% (vol/vol) paraformaldehyde for 10 minutes and labeled using the following primary antibodies- human anti-cTnT PE (R&D systems) and human anti-SMA APC (R&D systems) in 0.75% saponin. These were then incubated with goat-anti-mouse IgG conjugated to phycoerythrin and donkey-anti-rabbit IgG conjugated to allophycocyanin and analyzed using a BD FACSCANTO II (BD Biosciences) with FACSDiva software (BD Biosciences). Data analysis was performed using FlowJo software (Tree Star, Ashland, OR, USA).

**mRNA and miRNA sequencing analysis**

Total RNAs for 2 independent HFA and HFV samples were extracted using RNAeasy mini kit (Qiagen) (6). Two independent HAH total RNA samples were purchased commercially from Clontech and Agilent. Total RNAs for all other samples were extracted with miRNeasy mini kit (Qiagen) and were further DNAse treated with DNA-free kit (Ambion). Except IMR90iPSC-cardios where n=1 and EV samples (n=2) all other cardiomyocyte samples were obtained from 3 replicates. RNA and Small RNA libraries were prepared independently using Truseq library preparation kits (Illumina) following the manufacturer's protocols. The samples were sequenced on 28-70 million coverage. Sequence data for miRNAs were analyzed using miRDeep2 software (7). Raw sequences were first trimmed for any adapter and mapped to hg19 reference genome to produce arf files. These alignments are used to identify expression levels of known and novel miRNAs in sequence data. Differential expression analysis was done using edgeR 3.2.4 (8).For mRNA sequencing analysis, mRNA reads from 1yr old and 20 day old samples were mapped to hg19 reference genome using STAR version 2.3.0(9). BAM files produced by STAR were analyzed with Cufflinks version 2.1.1 run in de novo mode (10). Cufflinks output files as well as RefSeq gene models provided by UCSC were merged together using the Cuffmerge utility from the Cufflinks package. Apart from performing RNA sequencing analysis of two commercially available samples of HAH, We also located six state-of-the-art publicly available RNAseq samples (4 ventricular samples from Yang et al (11)., SRA accession numbers SRR830965,

SRR830966, SRR830967, SRR830968) and two whole-heart samples from (illumina body map 2.0 SRA accession numbers ERR030894, ERR030886) each with over 10 million reads per sample. While the sample preparation and sequencing protocols used for these samples were not identical to those used for the other samples in our study, the downstream bioinformatic analyses, starting from the raw fastq files downloaded from Sequence read archive (SRR830965, SRR830966, SRR830967, SRR830968, ERR030894, ERR030886, matched that used for our own sequence data as closely as possible. In particular, genome alignment and gene expression quantitation were done in the same way on all samples. All sequencing data related to this work is deposited in the Gene expression omnibus (GEO accession number GSE62913).

Gene and transcript abundance was estimated using Markov chain Monte Carlo to sample from a hierarchical Bayesian model. The model includes parameters separately capturing transcription and splicing rates at the sample, condition and experiment level. Under this model, estimates from transcripts with very low data are effectively shrunk towards each other to avoid spuriously highfold-change estimates that can occur when using simple read or fragment count
estimates. Expression estimates, measured in transcripts per million (TPM), and adjusted using upper quantile normalization (12), were generated for the Ensembl 74 gene annotation database(13). Separately, statistical significance of differential expression at the gene level was analyzed using DESeq (14). Both principle component analysis and hierarchical clustering were performed using log-transformed TPM gene expression estimates using R 3.0.2. Hierachical clustering used Euclidean distance as the metric. Heat map for the RNA sequencing data was generated using the edgeR version 3.2.4 (15) available in Bioconductor version 2.8 and for miRNA sequencing, data was generated using the multi experiment viewer (http://www.tm4.org)(16). Scatter plots were made using Microsoft Excel. Density plots were generated using R and. Kolmogorov-Smirnov test was used to calculate p-values (17). The miRNA-mRNA target and pathway analysis was done using IPA software (Ingenuity systems).

**Splice Variant analysis**

To define a set of differentially spliced genes, we looked for changes in isoform proportions, defined as an isoform's expression divided by the sum of the expression of all isoforms with the same transcription start site. To call differential splicing we looked for isoforms in which showed a specific and consistent ordering of the immature (day20 and EW CM) versus the mature (fetal, 1yr, and adult) samples with posterior probability > 0.75. Of all but three of the 80 isoforms called, this manifested as a consistent increase or decrease between immature and mature. To increase the chances of detecting changes in splicing dynamics the AceView gene annotations were used, which more liberally include alternate isoforms (18).

**miRNA and mRNA qPCR analysis**

Total RNAs were extracted with miRNeasy mini kit (Qiagen) or using trizol (Invitrogen). RNA was DNAse treated with DNA-free kit (Ambion). For RNA samples derived from hESC-CMs, human specific miR-let7g and mir-let7i taqman assays (Applied biosystems) were used for miRNA qPCRs following the manufacturer's protocol using RNU66 snoRNA as a loading control. Since, zebrafish and human let-7i share the same mature sequence, for all zebrafish miRNA qPCR, human specific let-7i taqman assay was used (Applied biosystems). For mRNA qPCR reverse transcription reaction was carried out using Omniscript RT kit (Qiagen). Human specific primers for CTNT, MYH7, RYR2, SERCA2 and GJA1 were based on Tulloch et al. and those for HCN4, KCNJ2, SCN5A, HMGA1, HMGA2, IRS2, INSR, LIN28, SLC27A6 and FABP2, CD36, PPARA, TRIM71, EGR1, CDKN1A were purchased from Real Time Primers. Fish primer sequences were as follows: b-actin-F-AAGCAGGAGTACGATGAGTC and R-TGGAGTCCTCAGATGCATTG;CTNT-F-GTCTGCACTTCGGCGGTTACA and R-GCACAGCATTCACTTCCTGA; CMLC2-F-GGAGAGAAGCTCAATGGCACA and R-GTCATTAGCAGCCTCTTGAACTCA; ATP2A2 F- GTGGATGATGGTGCTGAAGA and R-TGCAGGCCTAGACTGATGTG; CX43 F- TTCAAGTGCAATACCCAGCA and R-GGCCTTCAGCTCCTCTTCTT; RYR2B F- TCCAGCAGGACACTTGACAC and R-

CCAGATCCTCTCTGGGAACA. qPCR was performed using SYBR green chemistry and ABI 7300 Real time PCR system. Samples were normalized using GAPDH as a house keeping gene.

**Contractile force measurement**

Arrays of silicone microposts were fabricated out of polydimethylsiloxane (PDMS) via a previously-described double-casting process using soft lithography from a SU8 master (19). Each micropost within the arrays used for these studies was 6.45 μm in height, 2.3 μm in diameter, and the center to center spacing between adjacent posts was 6 μm. Prior to cell seeding, the tips of these microposts were stamped with 50 μg/ml of mouse laminin (Life Technologies), and the remaining surfaces of the array were fluorescently stained with BSA 594 and blocked with 0.2% Pluronic F-127 (in PBS) (20). CMs that were 1 week post pLKO-let7OE or EV lentiviral transfection, were seeded onto these arrays at a density of around 800,000 cells per substrate. One week following cell seeding, muscle twitches from individual hESCs-CMs were recorded with high-speed video microscopy within a live cell chamber at 37°C. These images were aquired using a Nikon Ti-E upright microscope with a 60X water-immersion objective and a Hammamatsu ORCA camera.A custom MATLAB code was then used to compare each time frame of this video, to a reference fluorescent image, taken at the base plane of the posts. The twitch force at each post was subsequently calculated by multiplying the deflection of the post by the post's bending stiffness (38 nN/μm). The total twitch force produced by the cell was then determined by adding together the twitch force measured at each post beneath the cell. The average spontaneous beating frequency of the cells was determined by locating the time at which each beat reaches a maximum in the total twitch force (using the same MATLAB code), calculating the frequency between each sequential beat: 1/ (time at which second beat occurs - time at which first beat occurs), and then averaging these frequencies across all of the measured twitch events.

**Generation and imaging of the ArcLight-reporter RUES2 stem-cell line.**

RUES2 cells stably expressing the voltage-sensitive protein ArcLight (21) were created by zinc-finger nuclease (ZFN)-mediated insertion of an expression cassette in the AAVS1 safe harbor locus as previously described (22-24). In brief, S249-Arclight cDNA (Addgene plasmid #36855) was polymerase chain reaction (PCR)–amplified with SpeI and AgeI restriction sites and was inserted into the corresponding sites of the donor plasmid pZDonor_AAVS1-CAG-mTmG-2A-Puro-pA(22). The resultant donor plasmid, pZDonor_AAVS1-CAG-Arclight-2A-puro-pA (referred to hereafter as AAVS1-Arclight) has AAVS1 homology arms flanking a transgene in which the constitutive CAG promoter drives expression of ArcLight and puromycin resistance (via a 2A linker). To insert this transgene into the AAVS1 locus (23), we co-transfected this donor plasmid as well as AAVS1 ZFNs into RUES2 hESCs followed by puromycin selection of successfully targeting clones. A candidate Arc-RUES2 clone was used for cardiomyocyte differentiation. Twenty one day old Arc-RUES2-CMs were transduced with let-7g and let7i lentivirus as described earlier. Two weeks after transduction, individual Arc-RUES2 CMs with and without let-7g OE were imaged using a confocal microscope (LSM-510, Carl Zeiss, Germany) operated in frame-scan mode. Fluorescence excitation was at 488 nm, and emission was passed through a 650-nm long-pass emission filter. Cardiomyocytes were field-stimulated at 0.5 Hz at room temperature while being maintained in Tyrodes buffer (NaCl 140mM, KCl 5.4mM, $MgCl_2$ 1.0mM, $CaCl_2$ 1.8mM, $NaH_2PO_4$ 0.33mM, glucose 5mM, HEPES 10mM, pH 7.4).

**Mitochondrial functional assay**

The Seahorse XF96 extracellular flux analyzer was used to assess mitochondrial function. The plates were pre-treated with 0.1% Gelatin. At around 20 days after differentiation, the cardiomyocytes (both empty vector control and let7 OE) were seeded onto the plates with a density of 30,000 cells per XF96 well (2,500/$mm^2$) to ensure about 90% surface coverage at the time of experiment. The seahorse assays were carried out 3 days after the seeding onto the XF96 well plate. One hour before the assay, culture media were exchanged for base media (unbuffered DMEM (Seahorse XF Assay Media)

supplemented with sodium pyruvate (Gibco/Invitrogen, 1mM) and with 25mM glucose (for MitoStress assay), 25mM glucose with 0.5mM Carnitine for Palmitate assay. Injection of substrates and inhibitors were applied during the measurements to achieve final concentrations of 4-(trifluoromethoxy) phenylhydrazone at 1 μM (FCCP; Seahorse Biosciences), oligomycin (2.5μM), antimycin (2.5μM) and rotenone (2.5μM) for MitoStress assay; 200mM palmitate or 33μM BSA, and 50μM Etomoxir (ETO) for palmitate assay. The OCR values were further normalized to the number of cells present in each well, quantified by the Hoechst staining (Hoechst 33342; Sigma-Aldrich) as measured using fluorescence at 355 nm excitation and 460 nm emission. Maximal OCR is defined as the change in OCR in response to FCCP compared to OCR after the addition of oligomycin. Cellular capacity to utilize Palmitate as an energy source was calculated as the OCR reduction after ETO addition from the second dose of palmitate addition. The reagents were from Sigma, unless otherwise indicated.

References


1. Laflamme MA & Murry CE (2011) Heart regeneration. *Nature* 473(7347):326-335.
2. Tulloch NL*, et al.* (2011) Growth of engineered human myocardium with mechanical loading and vascular coculture. *Circulation research* 109(1):47-59.
3. Paige SL*, et al.* (2012) A temporal chromatin signature in human embryonic stem cells identifies regulators of cardiac development. *Cell* 151(1):221-232.
4. Lian X*, et al.* (2012) Robust cardiomyocyte differentiation from human pluripotent stem cells via temporal modulation of canonical Wnt signaling. *Proceedings of the National Academy of Sciences of the United States of America* 109(27):E1848-1857.
5. Paige SL*, et al.* (2010) Endogenous Wnt/beta-catenin signaling is required for cardiac differentiation in human embryonic stem cells. *PloS one* 5(6):e11134.
6. Chong JJ*, et al.* (2013) Progenitor cells identified by PDGFR-alpha expression in the developing and diseased human heart. *Stem cells and development* 22(13):1932-1943.
7. Mackowiak SD (2011) Identification of novel and known miRNAs in deep-sequencing data with miRDeep2. *Current protocols in bioinformatics / editoral board, Andreas D. Baxevanis ... [et al.]* Chapter 12:Unit 12 10.
8. Robinson MD, McCarthy DJ, & Smyth GK (2010) edgeR: a Bioconductor package for differential expression analysis of digital gene expression data. *Bioinformatics* 26(1):139-140.
9. Dobin A*, et al.* (2013) STAR: ultrafast universal RNA-seq aligner. *Bioinformatics* 29(1):15-21.
10. Roberts A, Pimentel H, Trapnell C, & Pachter L (2011) Identification of novel transcripts in annotated genomes using RNA-Seq. *Bioinformatics* 27(17):2325-2329.
11. Yang KC*, et al.* (2014) Deep RNA sequencing reveals dynamic regulation of myocardial noncoding RNAs in failing human heart and remodeling with mechanical circulatory support. *Circulation* 129(9):1009-1021.

12. Bullard JH, Purdom E, Hansen KD, & Dudoit S (2010) Evaluation of statistical methods for normalization and differential expression in mRNA-Seq experiments. *BMC bioinformatics* 11:94.
13. Chung S*, et al.* (2007) Mitochondrial oxidative metabolism is required for the cardiac differentiation of stem cells. *Nature clinical practice. Cardiovascular medicine* 4 Suppl 1:S60-67.
14. Anders S & Huber W (2010) Differential expression analysis for sequence count data. *Genome biology* 11(10):R106.
15. McCall MN*, et al.* (2011) MicroRNA profiling of diverse endothelial cell types. *BMC medical genomics* 4:78.
16. Saeed AI*, et al.* (2003) TM4: a free, open-source system for microarray data management and analysis. *BioTechniques* 34(2):374-378.
17. Wang C, Dostanic S, Servant N, & Chalifour LE (2005) Egr-1 negatively regulates expression of the sodium-calcium exchanger-1 in cardiomyocytes in vitro and in vivo. *Cardiovascular research* 65(1):187-194.
18. Thierry-Mieg D & Thierry-Mieg J (2006) AceView: a comprehensive cDNA-supported gene and transcripts annotation. *Genome biology* 7 Suppl 1:S12 11-14.
19. Tan JL*, et al.* (2003) Cells lying on a bed of microneedles: an approach to isolate mechanical force. *Proceedings of the National Academy of Sciences of the United States of America* 100(4):1484-1489.
20. Sniadecki NJ & Chen CS (2007) Microfabricated silicone elastomeric post arrays for measuring traction forces of adherent cells. *Methods in cell biology* 83:313-328.
21. Jin L*, et al.* (2012) Single action potentials and subthreshold electrical events imaged in neurons with a fluorescent protein voltage probe. *Neuron* 75(5):779-785.
22. Gantz JA*, et al.* (Targeted genomic integration of a selectable floxed dual fluorescence reporter in human embryonic stem cells. *PLoS One* 7(10):e46971.
23. Hockemeyer D*, et al.* (2009) Efficient targeting of expressed and silent genes in human ESCs and iPSCs using zinc-finger nucleases. *Nat Biotechnol* 27(9):851-857.
24. Shiba Y*, et al.* (Human ES-cell-derived cardiomyocytes electrically couple and suppress arrhythmias in injured hearts. *Nature* 489(7415):322-325.

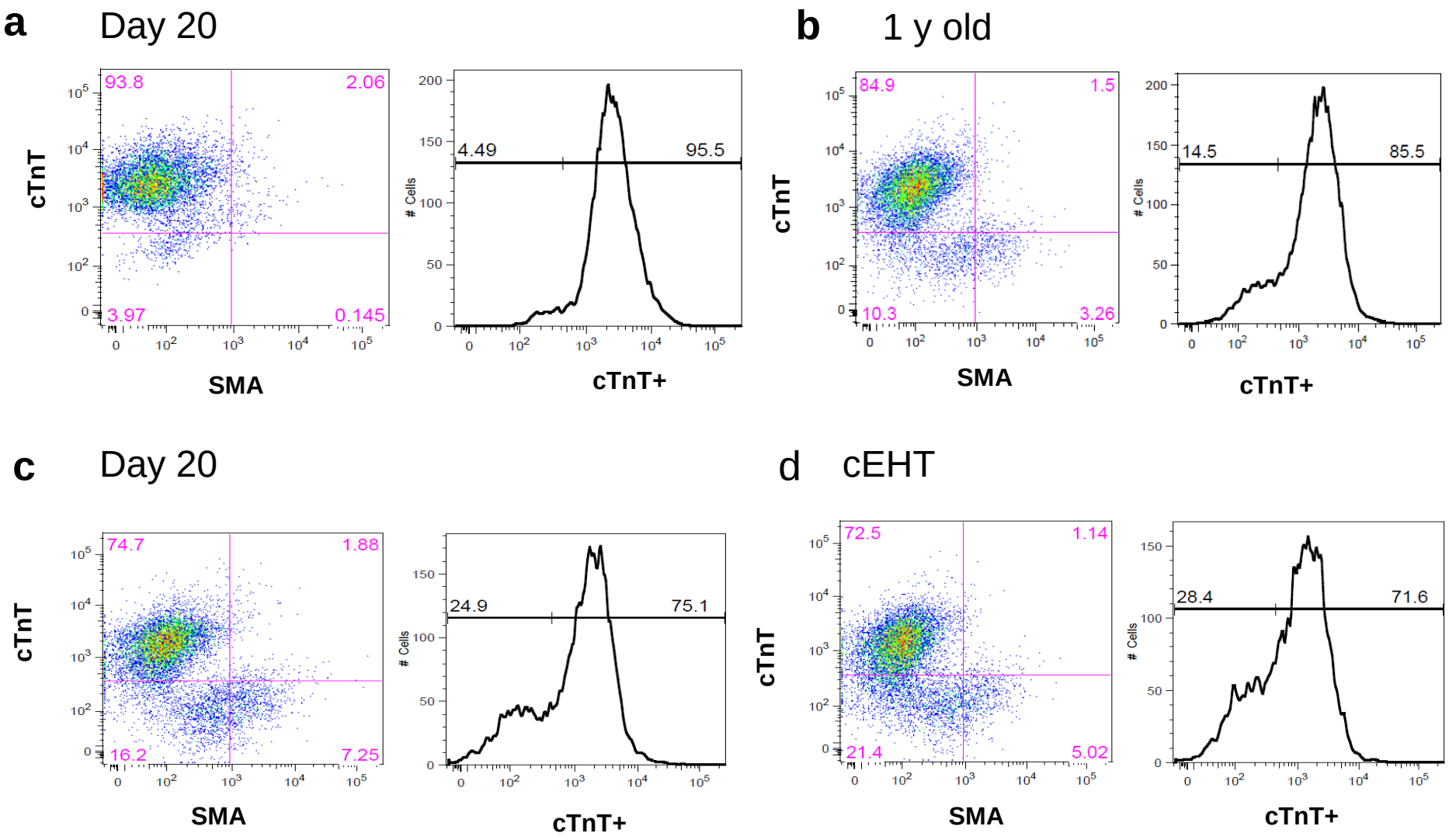


Figure S1. Representative flow cytometry analysis of hESC-CMs at day 20 (a and c), 1y old (b) cEHT (d) that demonstrated greater that 70% cardiac purity. cTnT: Cardiac troponin T; SMA: Smooth muscle actin.

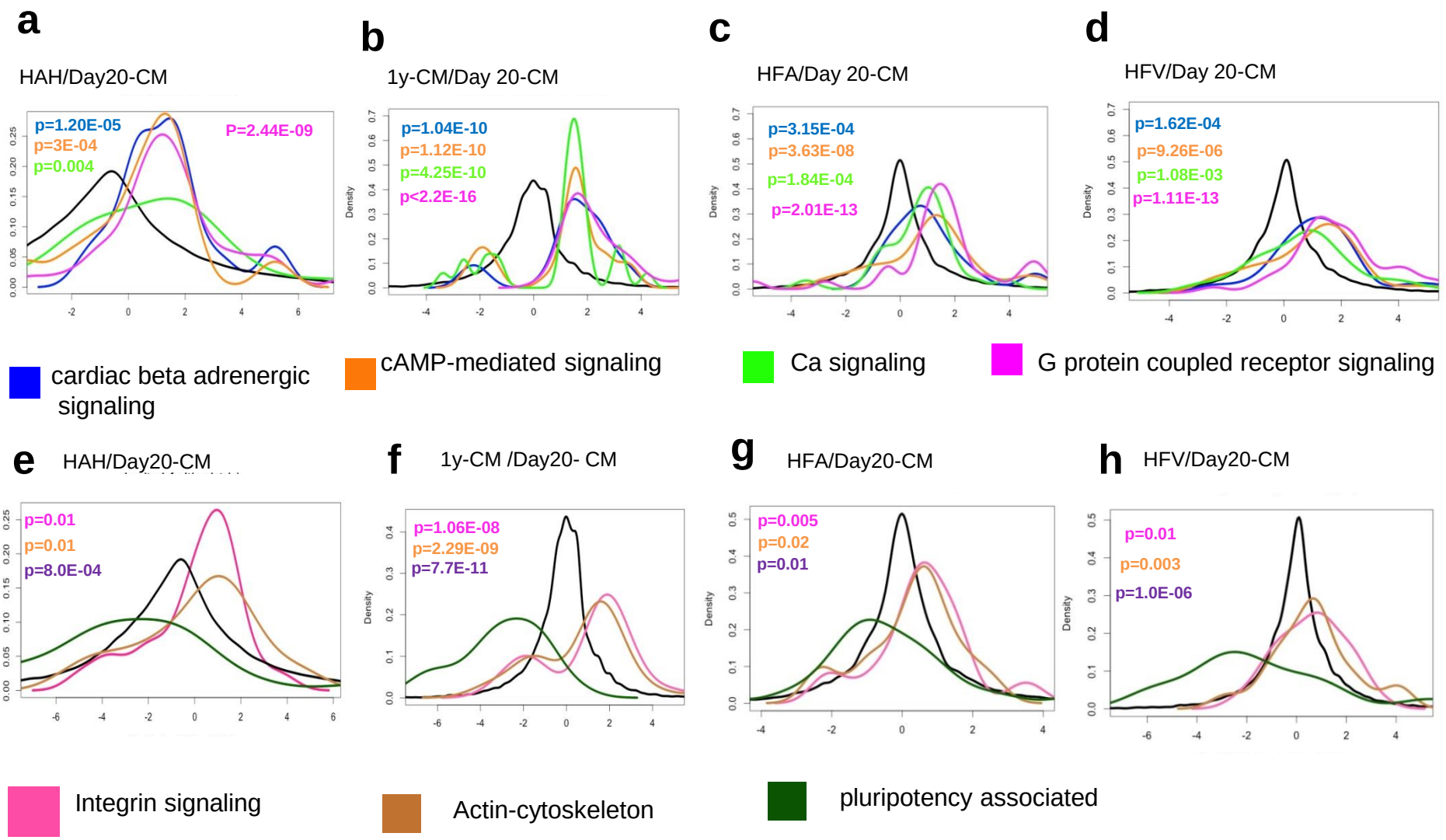


Figure S2. Density plots generated using fold change expression (x-axis indicates log2 fold change) of genes in HAH (a and e), 1y (b and f), HFA (c and g) and HFV (d and h) relative to day 20 cardiomyocytes. Black line indicates the entire gene set and colored lines indicated various pathways. Black line indicates expression of all genes. Colored lines towards the left and right side of the black line indicate down-regulation and up-regulation of pathways respectively.

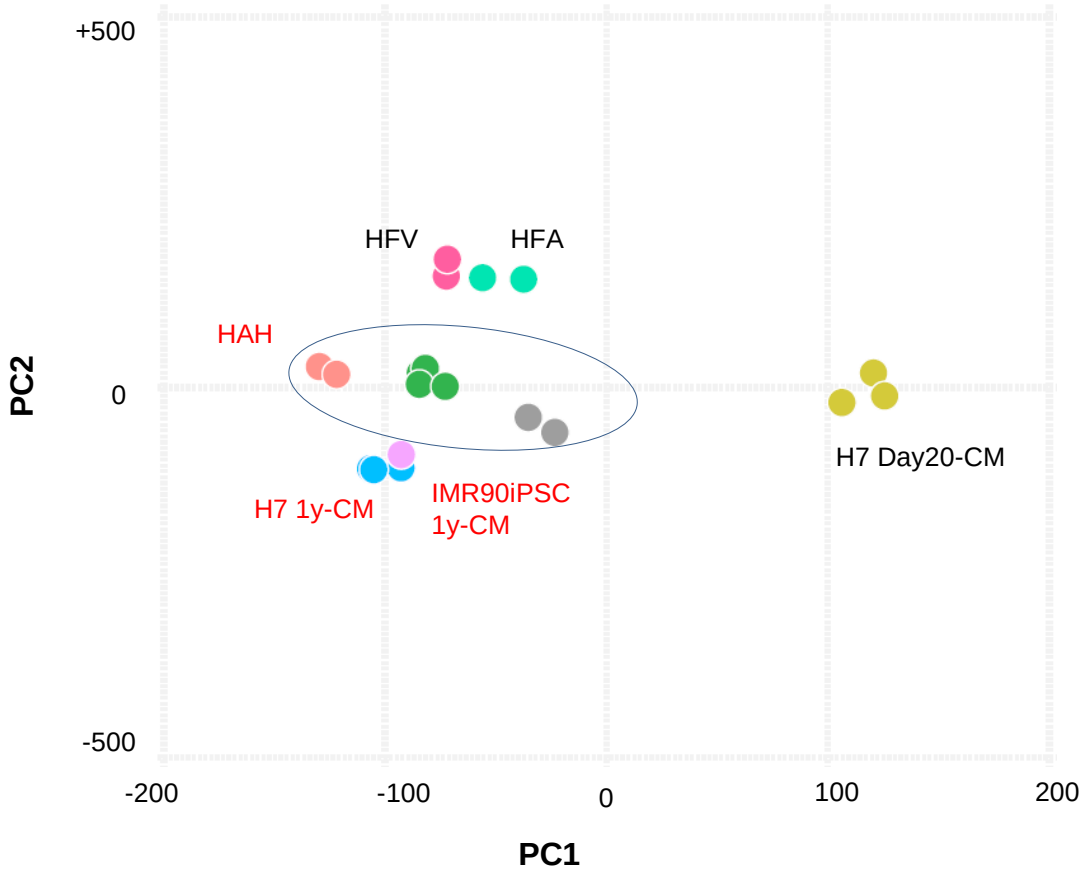


Figure S3. IMR90iPSCs-CMs and H7-CMs show similar changes in gene expression after prolonged culturing. 2D-PCA using all genes demonstrating the position of IMR90iPSC 1y-CMs relative to H7 1y-CMs, HAH, HFA and HFV samples.

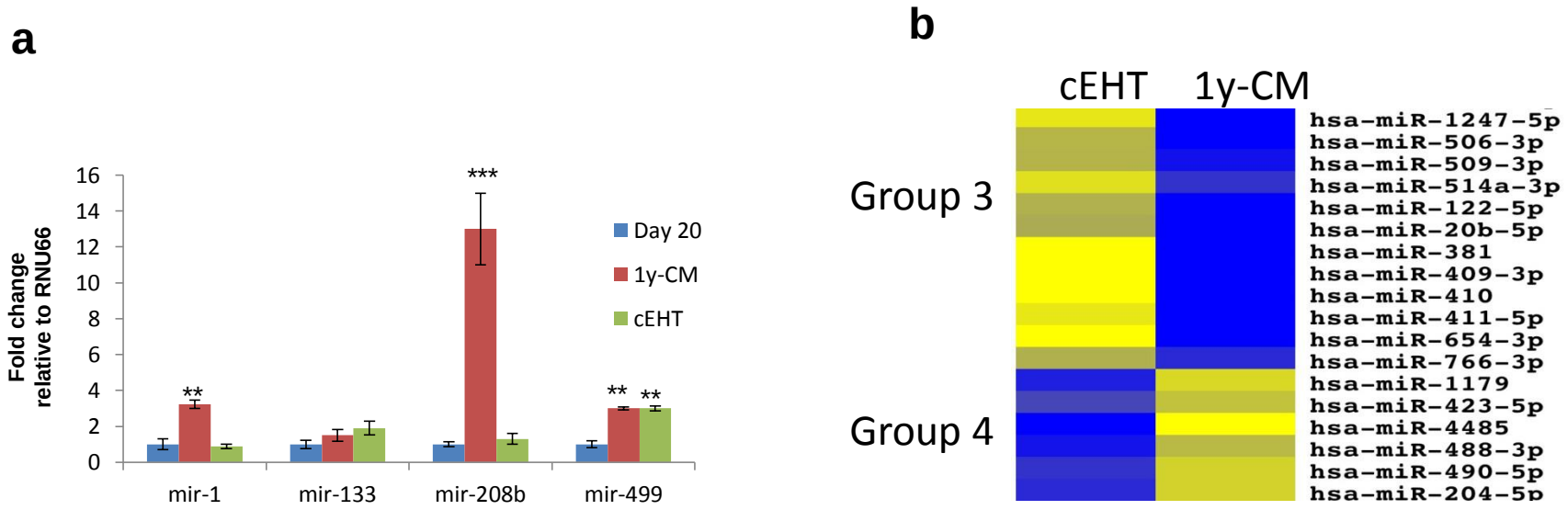


Figure S4. (a) qPCR analysis of myomiRs in 1y CMs and cEHTs relative to day 20 CMs (b) Heat map generated using multi expression viewer (http://www.tm4.org) includes fold changes of all significantly regulated miRNAs (FC≥2 and p≤0.001) that are common between 1y-CMs and cEHTs relative to day 20 CMs. Yellow and blue indicate up and down-regulation respectively. Groups 3 and 4 indicate miRNAs that are significantly up regulated in cEHT and down –regulated in 1y-CM and vice versa respectively.

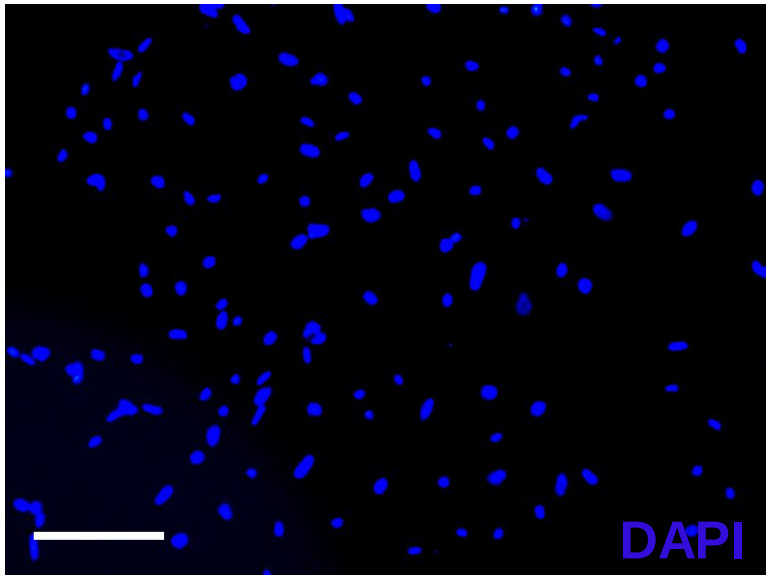


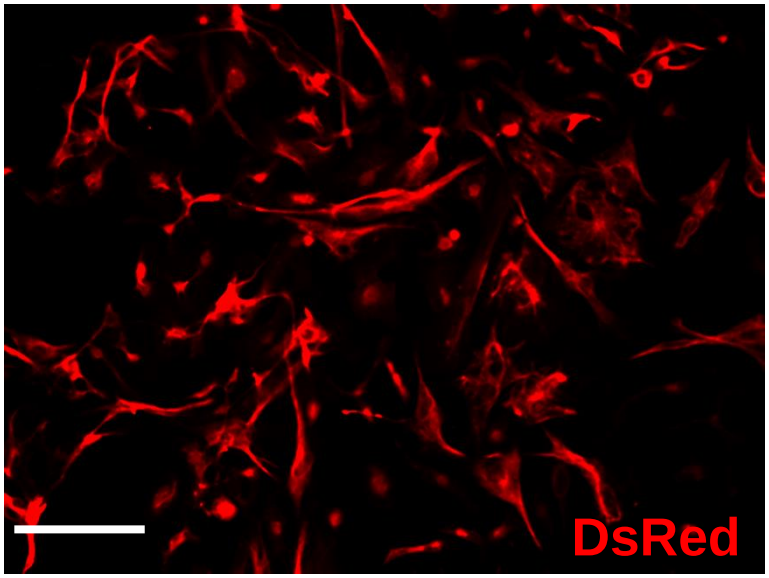


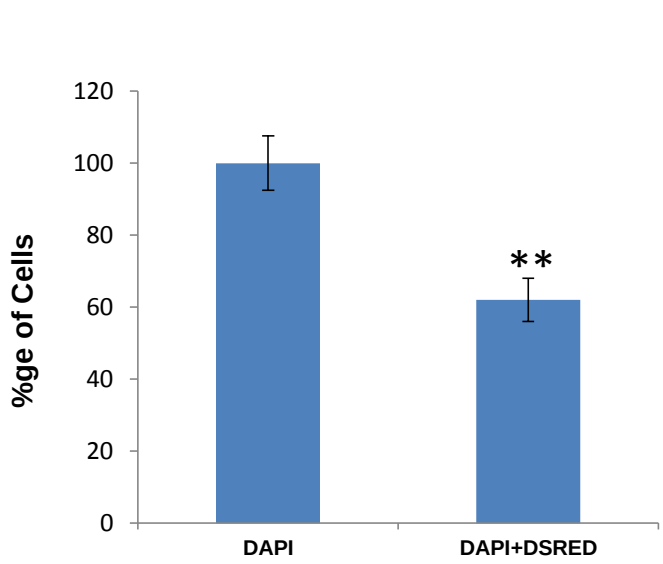


Figure S5. Transduction efficiency of pLKOlentiviral vector using DsRed reporter expression. Lentiviral transduction of the pLKO-DSred construct was carried out in cardiomyocytes at day 12 of differentiation run. DsRed reporter expression was analyzed at day 20. DAPI (a) and Ds red immuno fluorescence staining (b) of CMs that are at day 20 of directed differentiation run. Scale bar=50µm (c) Percentage of cells that has been successfully transduced. n= 100 cell from 3 independent transduction experiments. Means ± SEM are shown. **P≤ 0.05.

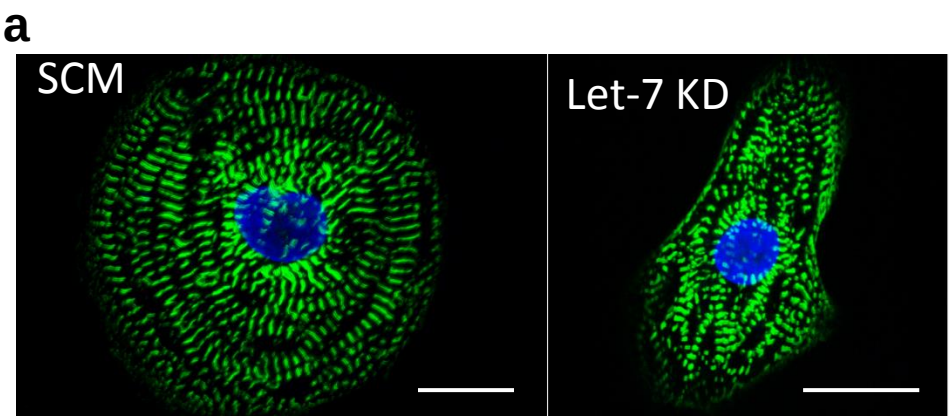


Figure S6. (a) α actinin (green) and DAPI (blue) staining of representative CMs treated with SCM control and let-7g antimir. Scale bar = 25µm. (b) Overexpression of let-7g using let-7g mimics results in increased expression of cardiac maturation makers. (c) (d) α actinin (green), a-actin (red) and DAPI (blue) staining of representative EV control, let-7i OE and let-7g OE CMs. Scale bar= 25µm.

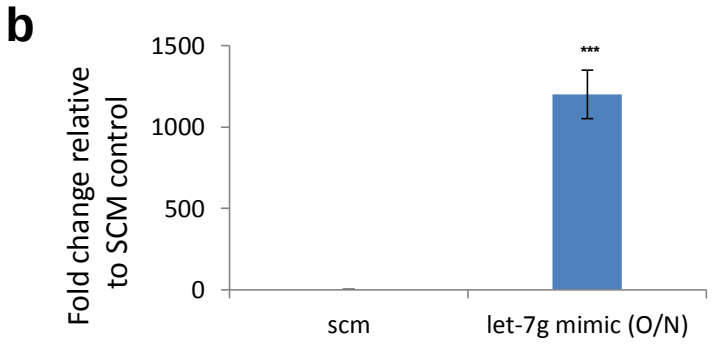


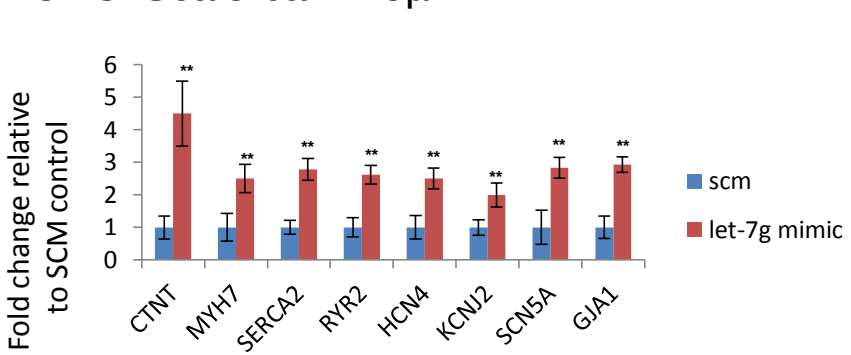


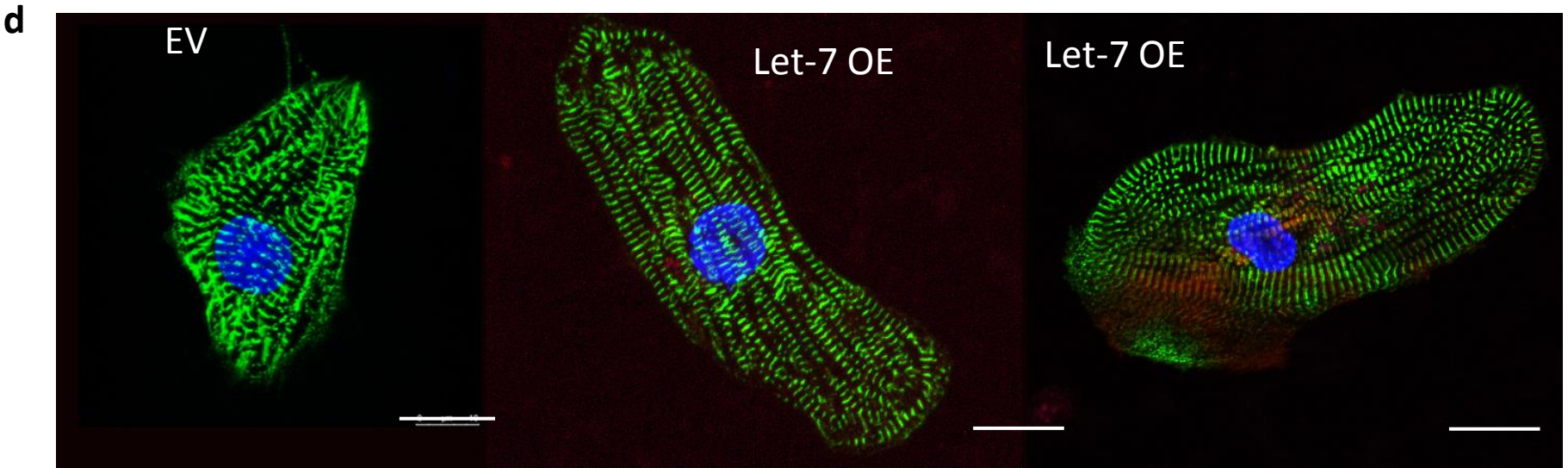

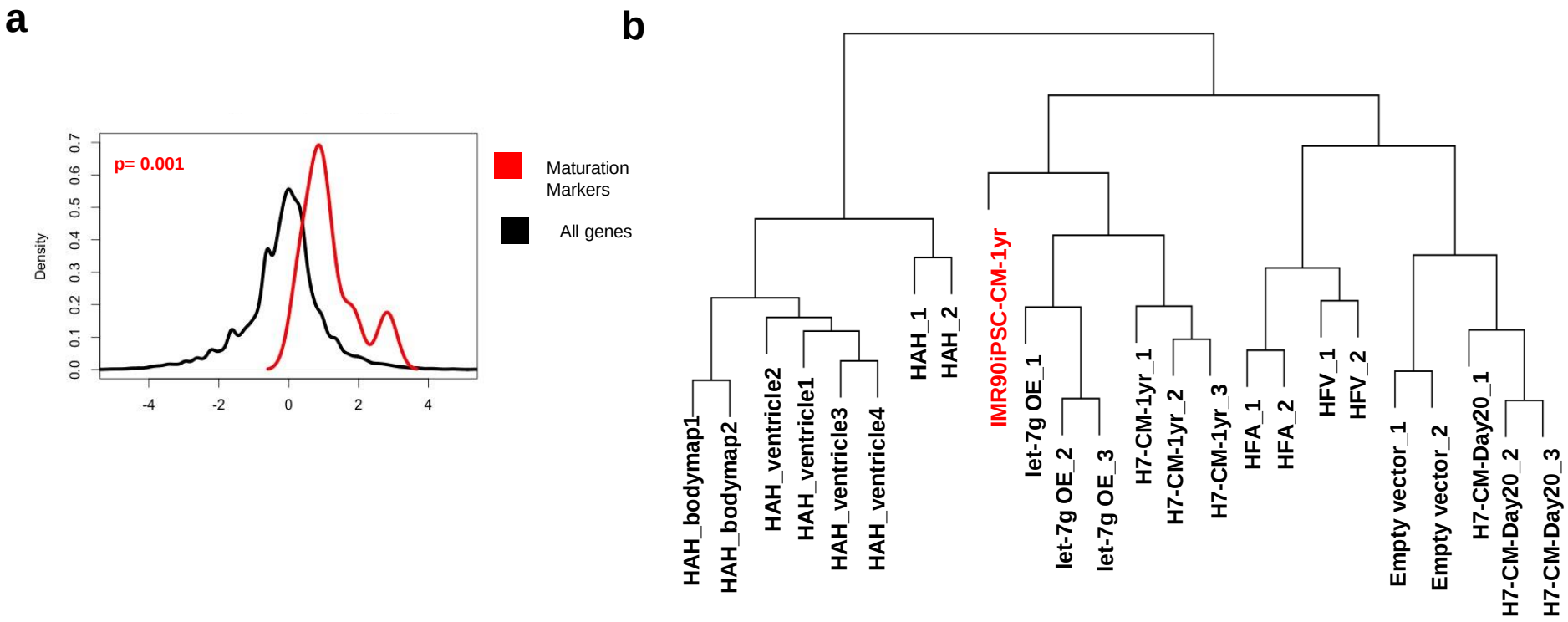


Figure S7. Overexpression of let-7 results in accelerated maturation. a) Density plots generated using fold change expression of maturation marker genes in let-7g OE CMs relative to EV control. b) An unbiased clustering analysis using expression data for genes from the 12 categories (see Fig.1) demonstrates that let-7 OE CMs cluster with H7 1y-CMs and IMR90iPSCs 1y-CMs.

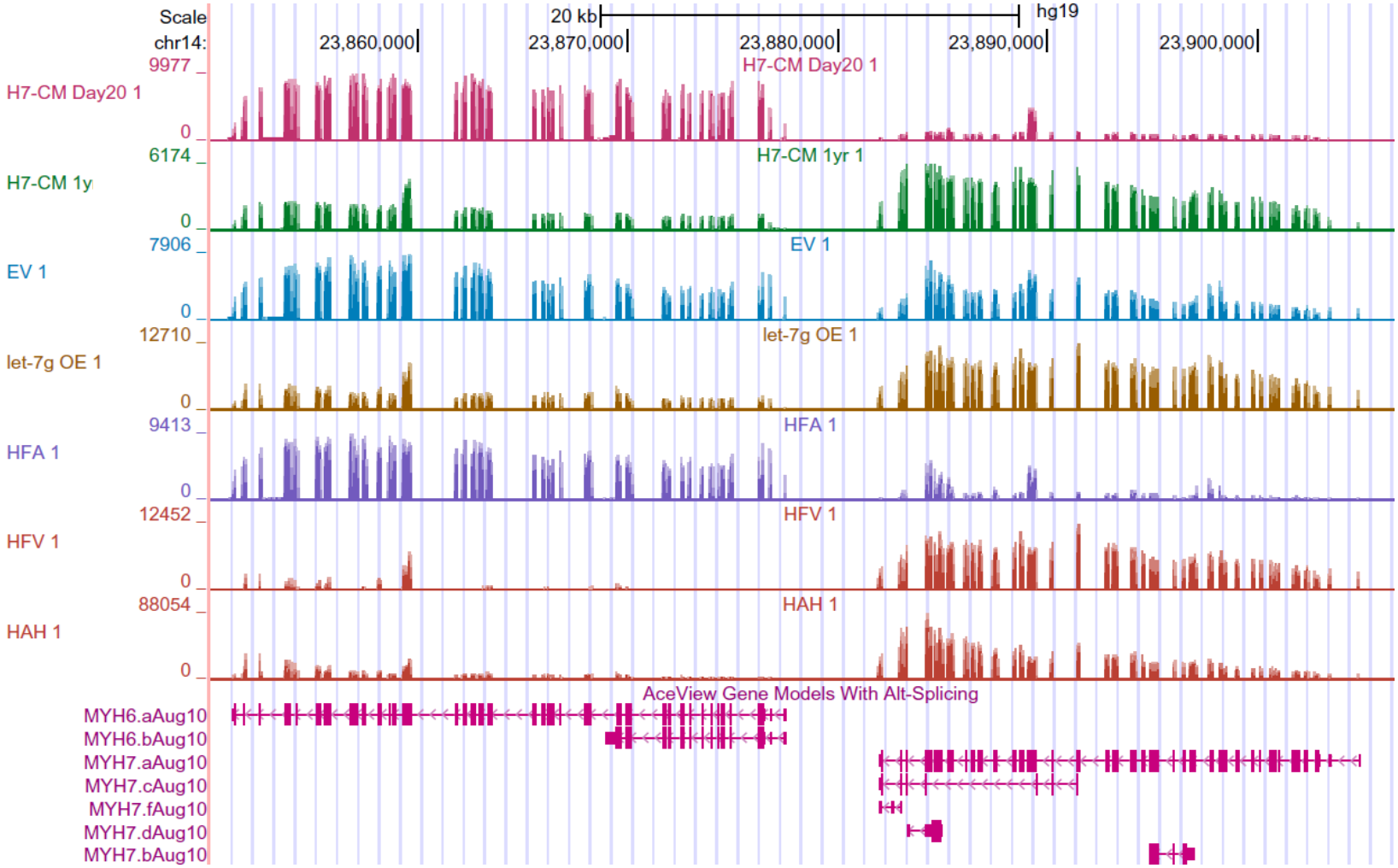


Figure S8. Let-7 OE in CMs results in isoform switch from myosin heavy chain (MyH) 6 (alpha; fast-twitch) to 7 (beta; slow-twitch) similar to that seen in 1y CMs, HAH and HFV sample. Screenshot from the UCSC genome browser showing detected isoform switching. The tracks show read coverage (i.e number of reads covering each position) on the y-axis for replicate 1 of the RNAseq data for each condition. Lower tracks give a representation of isoforms annotated by AceView.

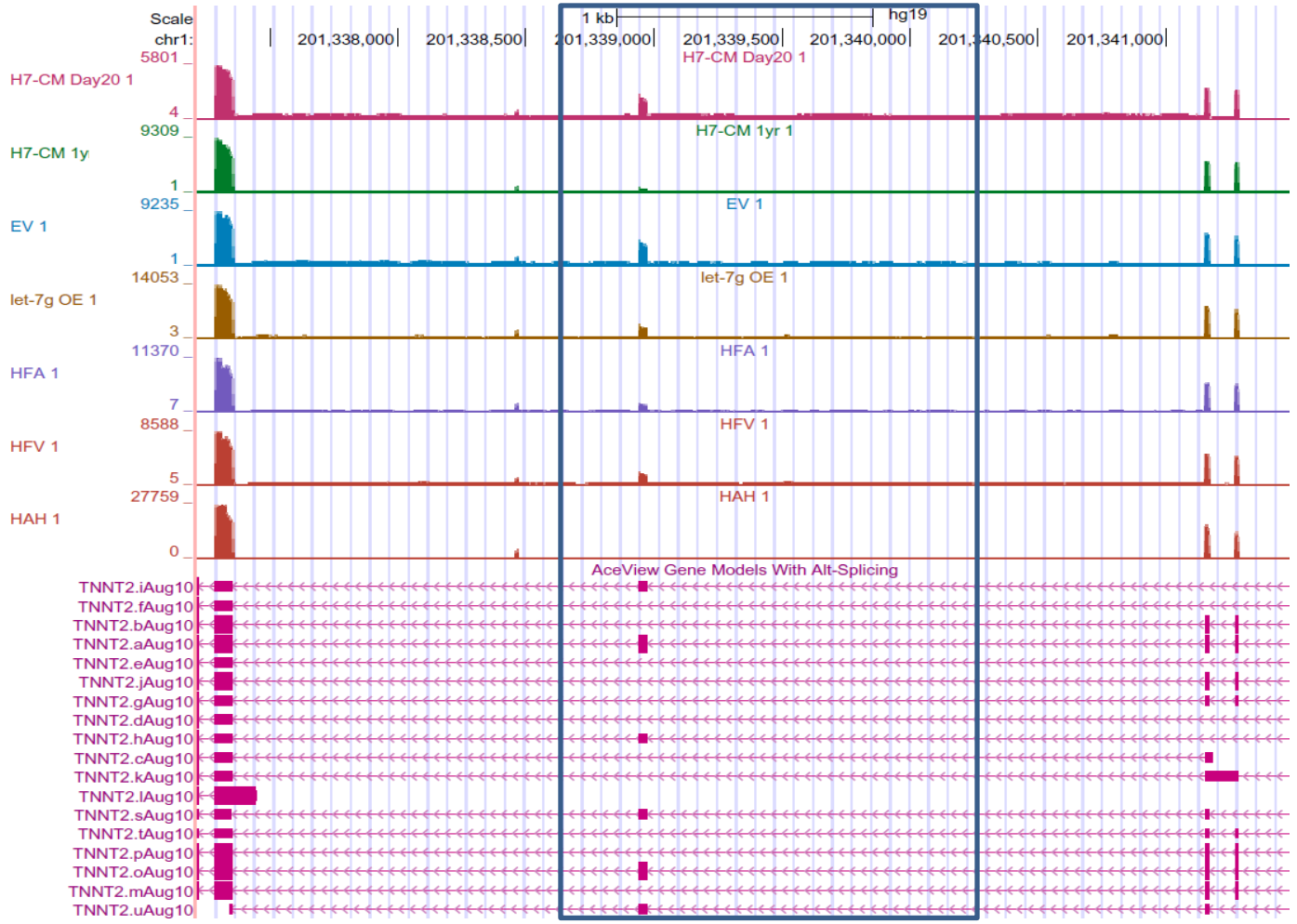


Figure S9. Putative alternative spliced variant of Cardiac Troponin T2 in let-7g OE CMs resembles that seen in 1y CMs, HAH, HFA and HFV samples. Screenshot from the UCSC genome browser focused on a portion of the Troponin T type 2 locus (TNNT2). One exon (marked in a box) is included in the TNNT2.a isoform, but excluded from the TNNT2.b isoform (AceView annotations; lower tracks).Read coverage (i.e., number of reads covering each position, shown in the y-axis for replicate 1 of each condition in the upper tracks) shows increased exclusion of this exon in let-7OE and other mature samples compared to day 20 and EV

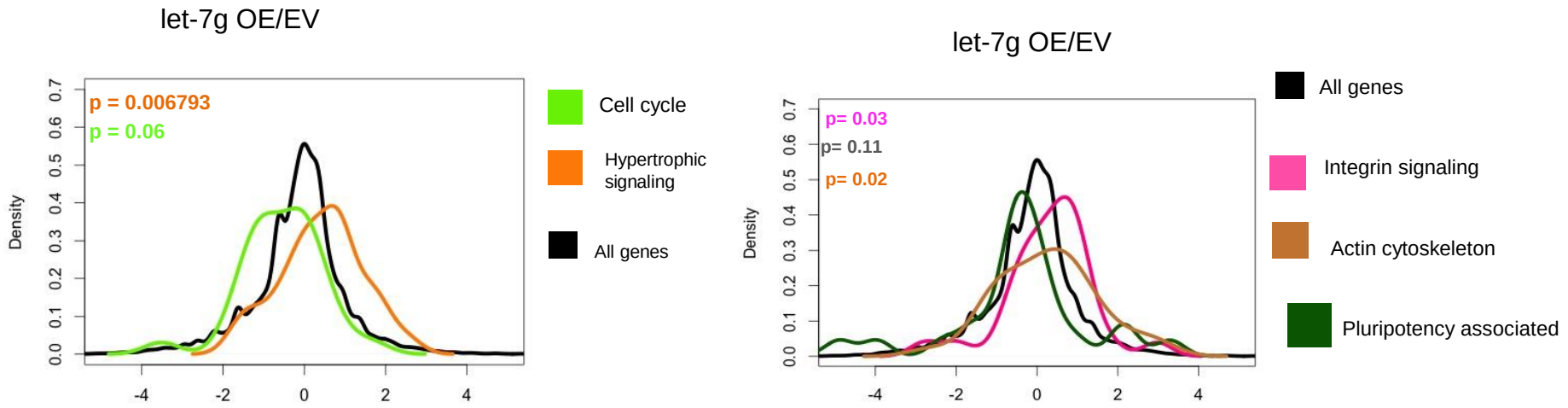


Figure S10. Let-7OE mimics gene expression profile observed during in vitro cardiac maturation. Density plots for representative categories of signaling pathways in let-7 OE CM samples. In each plot, black line indicates the entire gene set and the colored lines indicate the different categories.

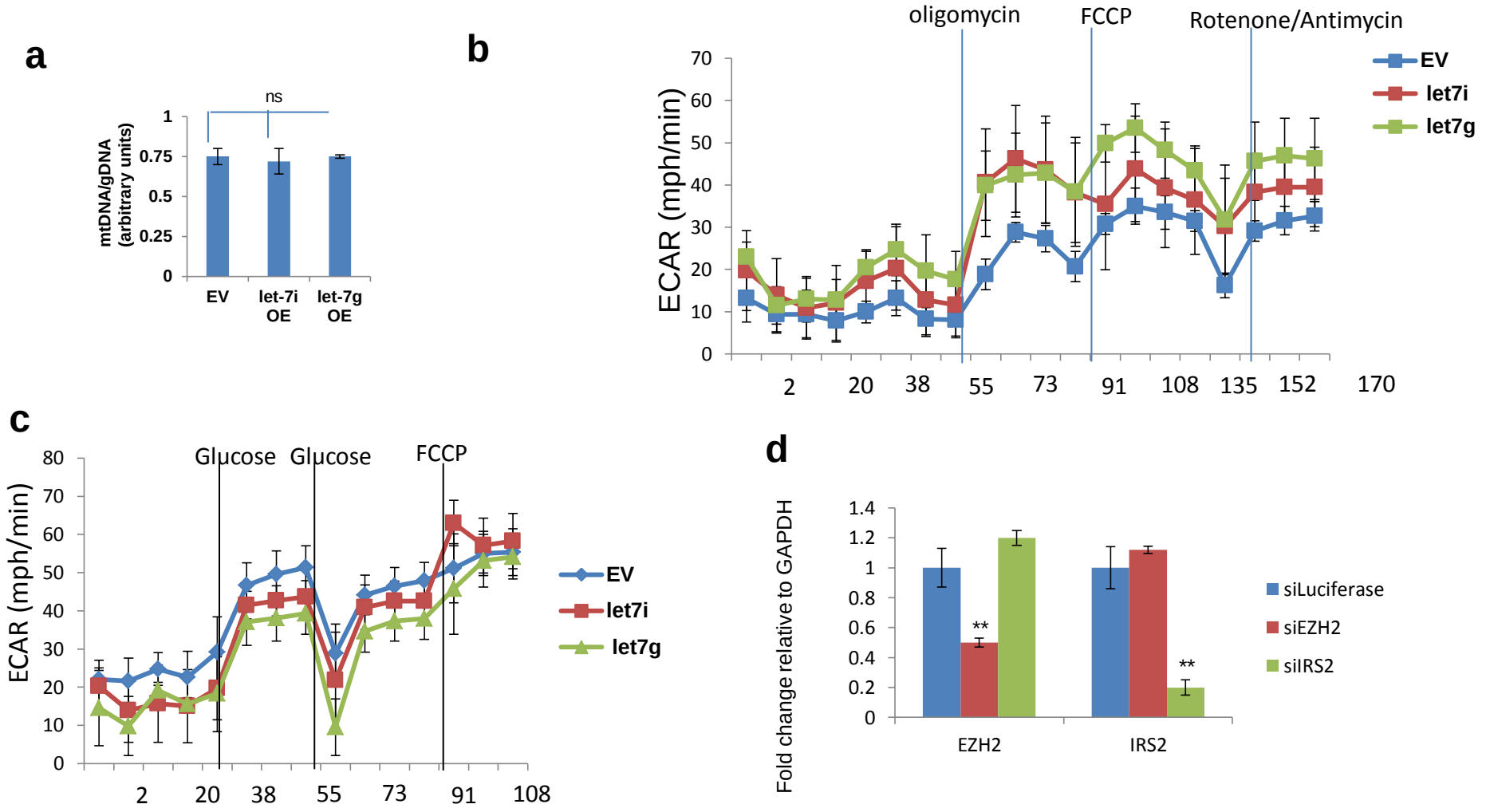


Figure S11. (a) mitochondrial DNA copy number was determined by measuring the ratio of MtDNA to genomic DNA using primers specific for mitochondrial DNA gene, Col (mtCol) and normalizing to chromosomal gene GAPDH Let-7 OE does not increase efficiency of glucose usage. (b-c) Quantification of ECAR change in EV control and let7-OE cardiomyocytes after (b) oligomycin addition in mito-stress assay. (c) glucose addition in glucose stress assay. In both the assays the values were normalized to the number of cells present in each well quantified by hoescht staining.(d) qPCR analysis of EZH2 and IRS2 in siEZH2-CMs and siIRS2- CMs.

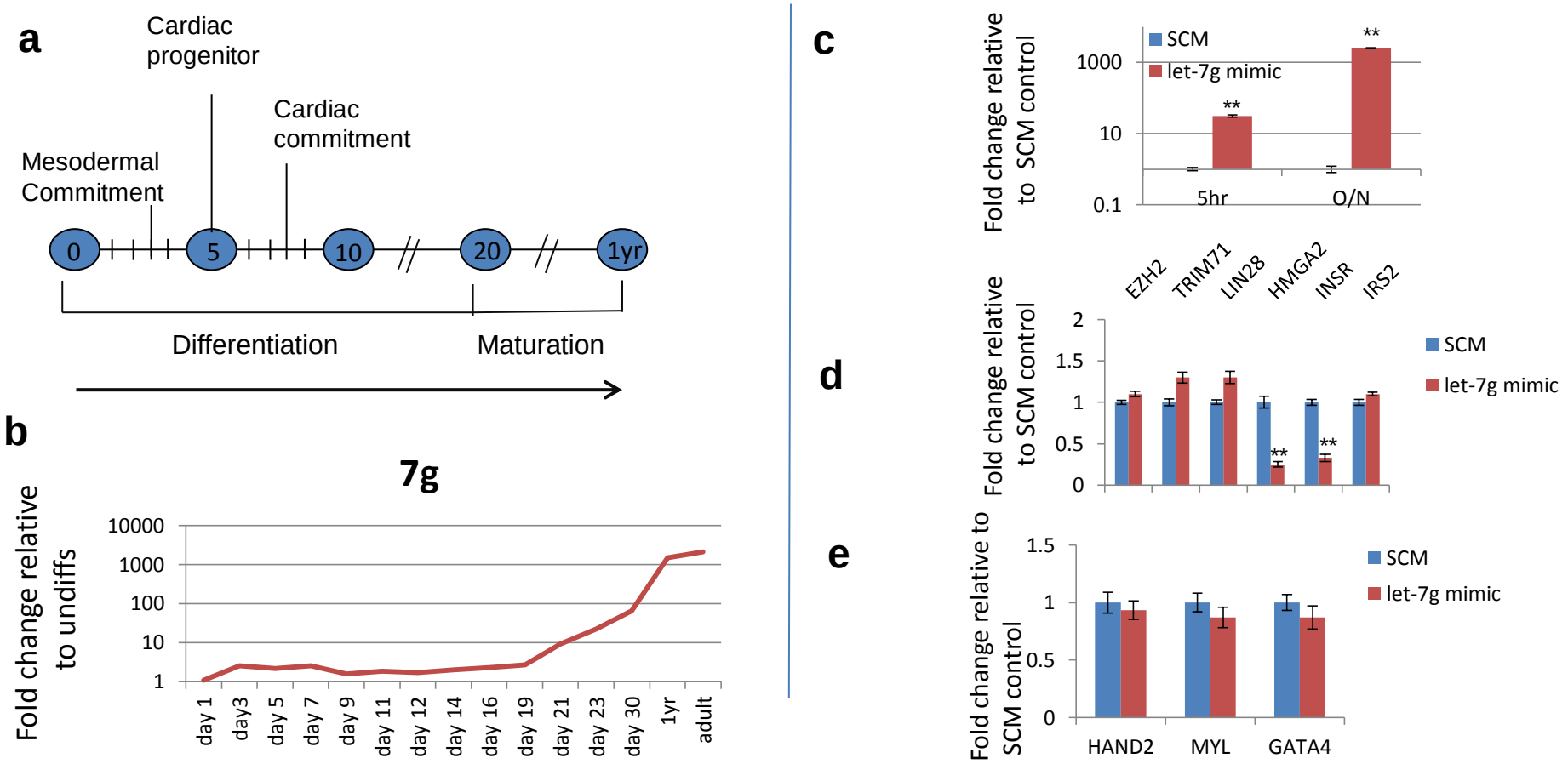


Figure S12. Let-7g does not have an essential role during early stages of human cardiac commitment in the *in-vitro* directed differentiation system. (a) Schematic representation of the time frame of our in-vitro differentiation system. Numbers in the circle indicate the days from induction with activin. (b) Time course of let-7g expression during differentiation and maturation of cardiac tissue from hESCs. The data is represented in comparison to the in-vivo derived adult heart samples. (c) Let-7g expression in cells transfected with scrambled control and let-7g mimic. (d) Expression of let-7 targets monitored at day 8 (e) Expression of cardiac markers monitored at day 8 (3 days after overnight transfections of the mimic and SCM control). Means ± SEM are shown. **P≤ 0.05 (Students t-test).

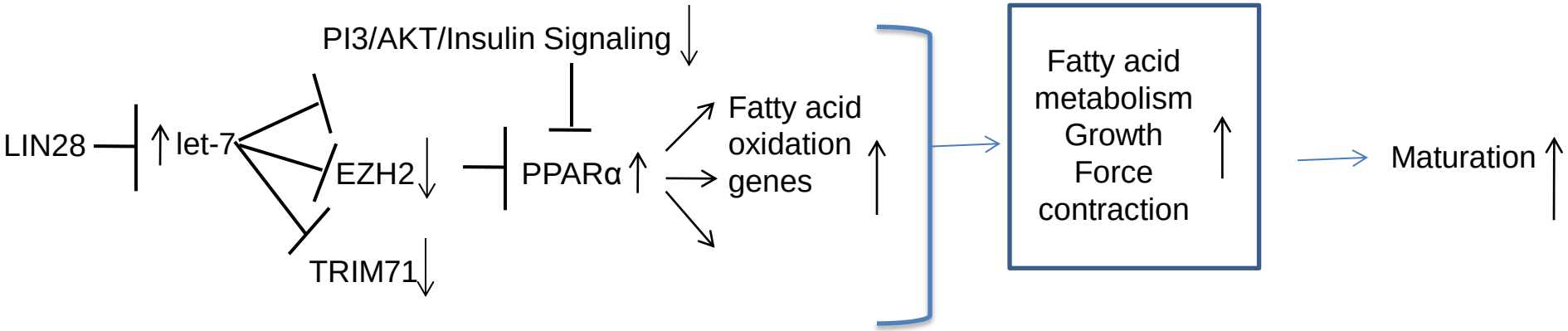


Figure S13. Proposed model for let-7 action in CM maturation. The arrows on the side of the each of the regulators indicate the direction of change when let-7 is induced.